2010

Accuracy of SRS dose delivery using the TomoTherapy Hi-Art System

Catherine Leigh Batte
Louisiana State University and Agricultural and Mechanical College, cbatt2@lsuhsc.edu

ACCURACY OF SRS DOSE DELIVERY USING THE TOMOTHERAPY HI-ART SYSTEM

A Thesis

Submitted to the Graduate Faculty of the
Louisiana State University and
Agricultural and Mechanical College
in partial fulfillment of the
requirements for the degree of
Master of Science

in

The Department of Physics and Astronomy

by
Catherine Leigh Batte
B.S., Centenary College of Louisiana, 2005
December 2010

ACKNOWLEDGMENTS

I would like to extend my thanks to my committee chair, Dr. Brent Parker for his help throughout the research process and in preparation of this thesis. I would also like to thank the members of my supervisory committee: Dr. Kenneth Hogstrom, Dr. Kip Matthews, Dr. Gabriela Gonzalez, Dr. Michael Price, and Dr. Robert Fields for their time and assistance on this research project. This research was supported in part by a research grant from TomoTherapy Inc. to Mary Bird Perkins Cancer Center, and I thank MBPCC for providing the physical resources necessary for this study. Finally, special thanks to my friends and family for their moral support through out graduate school.

TABLE OF CONTENTS

LIST OF TABLES

LIST OF FIGURES

ABSTRACT

Purpose: To quantify the accuracy and precision of both target positioning and dose delivery for intracranial radiosurgery delivered with the TomoTherapy Hi-Art System using a non-invasive immobilization device.

Methods: Techniques developed by Vinci *et al* (2007) were refined for the measurement of dose distributions in each principal plane using a CIRS head phantom. Pieces of Gafchromic EBT^2 film were cut and digitized using a template developed by Vinci *et al* (2007). A plan was created for a 2 cm diameter x 2 cm long cylindrical target in the TomoTherapy treatment planning system (TPS) version 3.2.1. Intentional misalignments of 5 mm in each of the principal directions were applied to the phantom prior to treatment delivery. The MVCT feature of the TomoTherapy Hi-Art system was used to correct for these misalignments, and then the treatment was delivered. Measured dose distributions (film) were registered to the calculated dose distributions (TPS planar dose) and compared.

Results: Alignment errors (displacement between the midpoints of the measured and calculated 70% dose points; mean ± standard deviation) were -0.15 ± 0.47 mm (range: -1.97 to 0.8 mm), -0.36 ± 0.56 mm (range: -1.25 to 0.63 mm), and -0.67 ± 0.93 mm (range: -3.04 to 0.90 mm) in the superior-inferior, anterior-posterior, and lateral directions, respectively. Positional errors of the 80% dose points in millimeters were 1.28 ± 0.91 (range: -0.09 to 3.62), -0.02 ± 0.96 (range: -2.24 to 1.72), -0.04 ± 0.62 (range: -1.24 to 1.25), 0.64 ± 0.52 (range: -0.35 to 1.55), 0.30 ± 0.52 (range: -1.57 to 1.28), and 0.60 ± 0.46 (range: -0.26 to 2.39) for the right, left, posterior, anterior, inferior, and superior directions, respectively.

Conclusions: Using a non-invasive immobilization device, 1.98 mm dose voxel size, and manual lateral couch positioning, the spatial accuracy of dose delivery with the TomoTherapy Hi•Art System was not within 1 mm as hypothesized.

CHAPTER 1: INTRODUCTION

1.1 BACKGROUND OF SRS

Stereotactic radiosurgery (SRS) was introduced in 1951 by the Swedish neurosurgeon Lars Leksell (Leksell, 1951). His work led to a non-invasive, single-fraction, radiotherapy method of treating intracranial malformations and lesions with results being equivalent to the surgical resection of the mass. This led to the term "stereotactic radiosurgery", indicating the procedure's biological effect within and immediately adjacent to the target volume. SRS achieves this result through the use of a single high dose of radiation, typically in the range of 12-20 Gy in conjunction with precise delivery. Due to the functional importance of intracranial tissues, high spatial accuracy is required of these high single-fraction doses because normal tissue complication rates increase dramatically with small increases in the volume irradiated at high fraction doses (Hall and Giaccia 2006).

Stereotactic radiosurgery (SRS) and stereotactic radiotherapy (SRT) are radiation therapy techniques where multiple beams with small field sizes are focused to treat small lesions, usually in the brain. SRS/SRT is currently used for the treatment of primary brain tumors, brain metastases, functional disorders, and vascular lesions. Imaging techniques accurate to within 1 mm are required to localize the target in the stereotactic frame. The AAPM Task Group 42 requirements for SRS are a positional accuracy of ±1mm and absorbed dose accuracy of ±5% (Schell, Bova et al 1995).

1.1.1 Traditional Frame-Based Radiosurgery/Radiotherapy

The foundation of SRS is accurate localization of the target within a well-defined coordinate system during treatment planning and delivery. Traditionally, this is accomplished by

attaching an invasive head ring to the patient to which a stereotactic localizer attaches for computed tomography (CT) imaging. Radio-opaque rods in the localizer allow the reference coordinate system to be defined in the CT coordinate system, and the tumor location is determined within this coordinate system.

(a) (b)

Figure 1.1 (a) CT stereotactic localizer attached to invasive head ring. Radio-opaque rods along the localization box define the stereotactic coordinate system in the treatment planning system. (b) Invasive stereotactic head ring. The head ring is rigidly attached to the patient's head and mounted to the treatment couch.

With SRS, the patient is initially imaged using a conventional CT scanner with the patient in the treatment position. A target localizer is attached to the invasive head ring which is mounted to the CT couch in order to immobilize the treatment anatomy. The stereotactic frame must be identified in the treatment planning system to define the stereotactic coordinate system. The relative locations of the fiducial rods are automatically located by the treatment planning system computer and define the steretactic coordinate system. For treatment, the head ring mounts to the treatment couch, and the couch is positioned so that the planned isocenter in the patient is coincident with the linac isocenter. SRS and SRT delivery options include multiple coplanar arcs with circular collimators, conformal fixed beams, conformal arc beams, and dynamic conformal arc beams.

The difference between SRS and SRT is that SRS is delivered in a single fraction while SRT is fractionated to spread the treatment over the course of multiple deliveries. SRS is the more precise (± 1 mm positional accuracy) treatment (Schell, Bova et al. 1995) because it is not subject to daily setup uncertainty. However, SRS lacks in that the patient does not get the additional biological benefits of fractionation. Fractionation allows increased sparing of normal tissue due to the repair of sublethal damage and reduction of acute reactions (Solberg, Selch et al. 1998).

SRT treatments involve multiple fractions using a removable, non-invasive immobilization device for treatment at the expense of increased setup uncertainty. Because the immobilization device must be positioned before each treatment, SRT may introduce interfraction positional variability. This increased variability leads to larger margins to cover the target volume due to the potential for increased patient setup uncertainty. One solution to improving setup accuracy for SRT treatments, and hence decreasing patient setup uncertainties, is image guidance.

1.2 IMAGE GUIDED RADIATION THERAPY

Image guided radiation therapy (IGRT) utilizes various imaging techniques immediately prior to treatment delivery to verify patient positioning. Until recently, image guidance typically was achieved using orthogonal portal films, but it has developed to include modern techniques using digital MV or kV systems.

The most common clinically utilized image-guidance systems can be divided into two groups: CT and planar-image based. Each can be gantry mounted or function as a stand alone system. Examples of gantry mounted CT include cone-beam MVCT (Siemens), cone-beam

kVCT (Varian or Elekta), and serial fan beam MVCT (TomoTherapy). An example of a CT as a separate system is a CT on rails (Siemens). Planar imaging utilizes x-rays, either megavoltage (MV) or kilovoltage (kV), directed at the patient immediately prior to treatment. The MV portal imagers and the kV imagers can either be gantry mounted (i.e. electronic portal imaging devices, EPIDs) or positioned independent of the gantry (i.e. kV X-ray tubes mounted elsewhere in the treatment room as is the Novalis ExacTrac system). Pre-treatment images are compared with reference images from the treatment planning system. Through this comparison, translations and rotations of the patient and/or couch necessary to align the patient with the planned setup are determined.

Using image-guided SRT, the patient treatment setup is directly compared to the planned setup, potentially negating the need for physical localization using a stereotactic frame. This assumes that the positioning accuracy of the IGRT system is at least as good as the traditional SRT positioning. The advancement of frameless SRT could have a significant impact on the accuracy of treatment delivery, and this improves the potential for reducing normal tissue complication from high-dose procedures (Holmes, Hudes et al. 2008).

1.3 BACKGROUND OF TOMOTHERAPY

"Tomotherapy" literally means slice therapy, and is a term derived from tomography (Mackie, Holmes et al. 1993). Tomotherapy is an application of intensity-modulated radiotherapy (IMRT) in which the patient is treated in the head-first, supine position slice by slice by an intensity-modulated, narrow-slit beam. Intensity-modulation is accomplished using a temporally-modulated binary multileaf collimator (MLC). Tomotherapy can be delivered in either a serial or helical fashion.

Serial tomotherapy, such as the Peacock system (Best Nomos, Pittsburgh, PA), mounts the temporally-modulated binary MLC to a conventional low energy megavoltage linear accelerator, and treatment is delivered to a narrow slice of the patient using arc rotation (Group 2001). The treatment is delivered serially to adjoining axial slices by moving the couch one to two slices at a time (Group 2001; Khan 2003). A potential problem with serial tomotherapy is the possibility of mismatch between adjacent slice pairs (Khan 2003). However, this is not a problem with a helical tomotherapy delivery unit, orginially proposed by Mackie *et al.* (1993). With helical tomotherapy, the linac head and gantry rotate around the patient at a constant angular velocity while the patient is translated through the bore at constant speed.

1.3.1 Background of TomoTherapy Hi-Art System

Helical tomotherapy was developed through the search for solutions to three major problems in radiation therapy: (1) the limitation of target dose that can be delivered due to the presence of neighboring sensitive structures; (2) verification of the correct beam shape and position while simultaneously ensuring that the patient is positioned correctly; (3) limitations in the safety of dynamic therapy due to the possibility of collision between the patient and the treatment unit (Mackie, Holmes et al. 1993). The TomoTherapy Hi-Art System (TomoTherapy Inc., Madison, WI) delivers IMRT in a manner analogous to the method utilized by a helical CT scanner when acquiring a patient image set (Group 2001). The unit uses CT slip-ring technology to deliver therapeutic radiation using a rotating fan beam which is modulated by a binary MLC. Beams are formed by the rapid opening and closing by the leaves of the MLC (see Figure 1.2). The binary MLC consists of 64 leaf pairs and planning of beams is done at fifty-one distinct

angles (spaced approximately every 7°) for each rotation (Mackie, Olivera et al. 2003). The time each of the 64 leaves remains open per projection is optimized to achieve IMRT delivery.

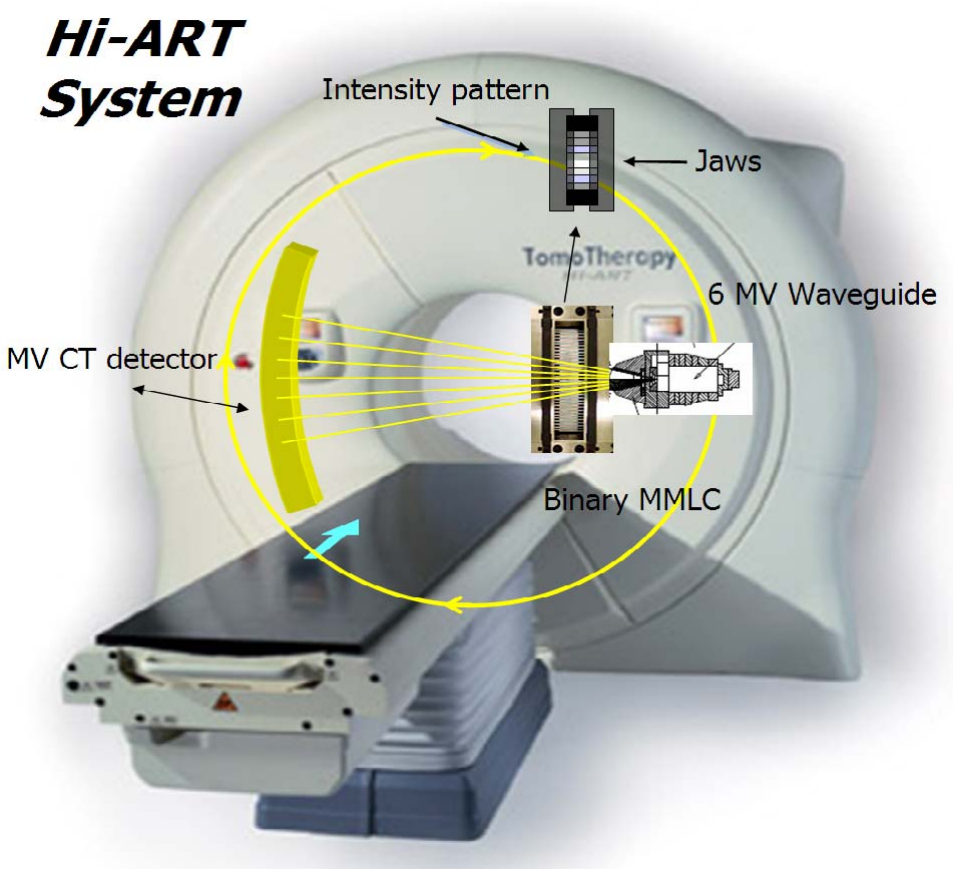

Figure 1.2 TomoTherapy Hi-Art treatment unit. Shows the linac source and the MVCT detector arrary. Depicts the manner in which TomoTherapy delivers treatments helically. (from Hesston 2009)

This study focuses on image guidance using the MVCT feature of the TomoTherapy Hi-Art System. The TomoTherapy Hi-Art unit utilizes a xenon ion chamber CT detector array on board to acquire a transmission signal from the linac beam (Mackie, Olivera et al. 2003). The same linac source used for treatment (6 MV) can also produce a low-intensity 3.5 MV (nominal) energy x-ray beam for imaging. TomoTherapy has 3 scan acquisition slice thickness options fine (2 mm), normal (4 mm), and coarse (6 mm). The images acquired pre-treatment can be automatically registered to the radiotherapy planning kVCT using either bony anatomy or soft

tissue and bony anatomy. Automatic registration is accomplished by Mutual Information (MI, or the full image technique) or by a variation of MI developed by Ruchala *et al*. called extracted feature fusion. EFF is a voxel-based registration algorithm in which the parameters are determined by the optimization of a similarity measure that depends only on those voxels in the reconstructed image with values above a threshold of 1.1 or 0.3 g/cm^3, typical of bone or bone and tissue, respectively (Boswell, Tome et al. 2006). By registering the image sets, the translations and rotations required to align the patient with the planned patient setup, can be applied prior to treatment delivery.

1.3.2 Therapy Delivery Differences

Helical TomoTherapy delivers radiation utilizing many more beam angles compared to conventional radiotherapy and delivers the radiation slice by slice. This allows for better dose conformation to complex-shaped targets and for targets close to critical structures. However, compared to conventional IMRT, larger volumes of normal tissue will receive low doses. This is believed to potentially contribute to secondary cancer risks. To restrict the normal tissue dose, intracranial SRS treatments are typically carried out using noncoplanar beam arcs. However, helical tomotherapy delivery is limited to coplanar beams because the TomoTherapy couch can not rotate. Consequently, TomoTherapy delivers a higher dose to nontarget regions (Holmes, Hudes et al. 2008). However, TomoTherapy provides excellent dose conformation regardless of the complexity of the target as well as allows for simultaneous treatment of multiple targets (Holmes, Hudes et al. 2008).

1.4 MOTIVATION FOR RESEARCH

SRS using an invasive head frame is a very precise treatment option (± 1mm), but it does not afford the patient the additional benefits of fractionation. Conversely, non-invasive immobilization devices used for fractionated treatments allow increased interfraction and intrafraction positional variability. IGRT can be employed to improve the setup accuracy using a non-invasive immobilization system. With the use of IGRT, it is theoretically possible to achieve treatment accuracy typical of SRS assuming there is no intrafraction motion.

Increased certainty of tumor location will make frameless radiosurgery using TomoTherapy more clinically applicable. For frameless radiosurgery, there is a potential for intrafraction motion. However, this is reduced by using a thermoplastic mask, custom fit to each patient, for immobilization. The possibility of interfraction setup variability requires a larger margin and planned target volume (PTV) for treatment. Although this margin ensures adequate target dose coverage, it also results in a larger volume of normal tissue receiving therapeutic doses. Using the TomoTherapy MVCT, interfraction error can be reduced or eliminated, negating the need for an expanded PTV, thus reducing the volume of normal tissue irradiated.

The current literature investigating SRS using TomoTherapy utilizes invasive immobilization for the treatment of intracranial lesions. Holmes, Hudes *et al*. (2008) determined that the accuracy of the TomoTherapy Hi-Art II system for localizing dose to a small target is within the accepted specification of 2 to 2.4 mm for SRS treatments using image-guided IMRT. Soisson, Sobering *et al*. (2009) utilized an anthropomorphic head phantom and an intracranial stereotactic positioning system to test the ability of the MVCT to detect a known shift applied to an anthropomorphic head phantom; it was determined the TomoTherapy Hi-Art system was

capable of sub millimeter setup accuracy. Currently there is a lack of information regarding the viability of frameless radiosurgery.

Frameless radiosurgery using TomoTherapy will afford physicians at smaller community facilities without a dedicated SRS unit the option to deliver stereotactic therapy. Because of the typical time constraints associated with conventional SRS (i.e. invasive head frame), inverse treatment planning and optimization with TomoTherapy is not usually a viable option (Fuss and Salter 2007). However, frameless radiosurgery using TomoTherapy would provide physicians with the ability to use the inverse planning and treatment optimization because preparation of the plan could be done 1 to 2 days prior to the treatment date. This study will focus on quantifying the accuracy and precision of both target positioning and dose delivery for intracranial radiosurgery delivered with the TomoTherapy Hi-Art system using a non-invasive immobilization device.

1.5 HYPOTHESIS AND SPECIFIC AIMS

The hypothesis of this project is that treatment delivery using the MVCT image guidance feature of the TomoTherapy Hi-Art System at MBPCC has a positional dose delivery accuracy within ± 1 mm for a cranial PTV in an anthropomorphic head phantom.

Two aims were completed to test this hypothesis:

Aim 1. Refine measurement and analysis techniques developed by Vinci et al (2008).

Develop procedure for comparing measured (radiochromic film) and calculated (TomoTherapy TPS) planar dose distributions in the cranium of an anthropomorphic head phantom.

Aim 2. Determine the accuracy and precision of dose delivery for TomoTherapy IGRT.

Intentionally misalign the phantom by known offsets from isocenter prior to treatment and use the TomoTherapy MVCT image registration procedure to align the phantom prior to delivering the planned treatment. Compare measured dose distributions with calculated dose distributions from the TPS to quantify spatial accuracy of dose delivery using TomoTherapy IGRT.

1.6 REFERENCES

Boswell, S., W. Tome, et al. (2006). "Automatic Registration of Megavoltage to Kilovoltage CT Images in Helical Tomotherapy: An Evaluation of the Setup Verification Process for the Special Case of a Rigid Head Phantom." Medical Physics **33**(11): 4395 – 4404.

Childress, N.L., L.Dong, et al. (2002). "Rapid Radiographic Film Calibration for IMRT Verification Using Automated MLC Fields." Medical Physics **29**: 2384 – 2390.

Fuss, M. and B.J. Salter (2007). "Intensity-Modulated Radiosurgery: Improving Dose Gradients and Maximum Dose Using Post Inverse-Optimization Interactive Dose Shaping." Technology in Cancer Research and Treatment **6**(3): 197 – 203.

Group, I. M.R.T.C.W. (2001). "Intensity-Modulated Radiotherapy: Current Status and Issues of Interest." International Journal of Radiation Oncology Biology Physics **51**(4): 880 – 914.

Hesston, R. (2009). Dosimetric Evaluation of a Delivery Verification and Dose Reconstruction Method for Helical TomoTherapy. Physics and Astronomy. Baton Rouge, Louisiana State University and Agricultural and Mechanical College. **Master of Science**: 87.

Holmes, T. W., R. Hudes, et al.(2008). "Stereotactic Image-Guided Intensity Modulated Radiotherapy Using the Hi-Art II Helical Tomotherapy System." Medical Dosimetry **33**(2): 135 – 148.

Khan, F.M. (2003). Tomotherapy. The Physics of Radiation Therapy. Philadelphia, Lippincott Williams & Wilkins.

Mackie, T.R., T. Holmes, et al. (1993). "Tomotherapy: A New Concept for the Delivery of Dynamic Conformal Radiotherapy." Medical Physics **20**(6): 1709 – 1719.

Mackie, T.R., G.H. Olivera, et al. (2003). Helical Tomotherapy. Intensity-Modulated Radiation Therapy – The State of the Art. J. Palta and R. Mackie. Madision, Medical Physics Publishing: 247 – 284.

K. Ruchala, G.H. Olivera, and J. Kapatoes. (2002). "Limited-Data Image Registration for Radiotherapy Positioning and Verification." International Journal of Radiation Oncology Biology Physics. **54**: 592 – 605.

Schnell, M.C., F. J. Bova, et al. (1995). "Stereotactic Radiosurgery Report of Task Group 42." Medical Physics **June 1995**: 1 – 83.

Soisson, E. T., G. Sobering, et al. (2009). "Quality Assurance Of An Image Guided Intracranial Stereotactic Positioning System." Technology in Cancer Research and Treatment **8**(1):39 – 49.

Solberg, T., M. Selch, et al. (1998). "Fractionated Stereotactic Radiotherapy: Rationale and Methods." Medical Dosimetry **23**: 209 – 219.

Vinci, J.P., K. R. Hogstrom, et al. (2008). "Accuracy of Cranial Coplanar Beam Therapy Using an Oblique, Stereoscopic X-Ray Image Guidance System." Medical Physics **35**(8): 3809 – 3819.

CHAPTER 2: METHODS AND MATERIALS

2.1 TREATMENT PLAN DESIGN

2.1.1 Anthropomorphic Head Phantom

Anthropomorphic head phantoms have been used extensively for clinical treatment plan verification (Holmes, Hudes et al. 2008; Vinci, Hogstrom et al. 2008; Soisson, Sobering et al. 2009). The CIRS (Norwalk, VA) Model 605 radiosurgery anthropomorphic head phantom was used as a patient surrogate to evaluate the delivery accuracy of TomoTherapy IGRT. This phantom was selected for its similarity to human anatomy with regard to radiation interactions. The CIRS 605 phantom reproduces the attenuation characteristics of a human head with 1% accuracy for energies of 50 keV to 25 MeV (CIRS Radiosurgery Head Phantom Model 605 Specification Sheet). A comparison between the linear attenuation coefficients of the phantom and those of an "average" human head in the energy range of 0.04 MeV to 30 MeV, provided by CIRS, is shown in Appendix A for the five phantom materials – soft tissue, bone, spinal discs, spinal cord, and brain tissue. Figure 2.1 shows the phantom assembled as well as the disassembled phantom with its film dosimetry insert exposed.

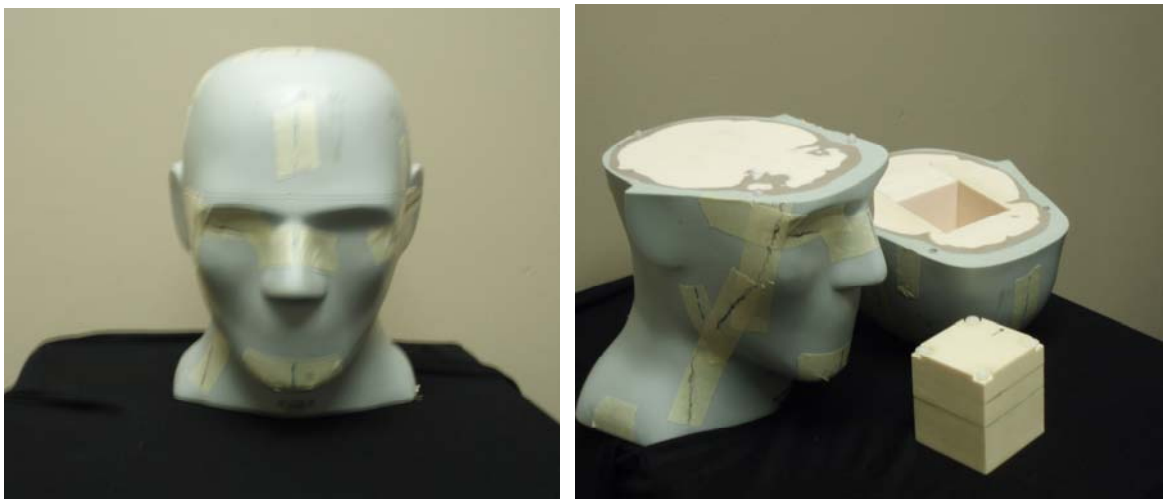

(a) (b)

Figure 2.1: (a) CIRS Model 605 Head Phantom. (b) Film phantom measurement system with film block.

A cubic film block (6.35 cm on each side) capable of holding film at two locations (25% and 50% across the block width) was used in this study (see Figure 2.2 (a)). For all measurements in this study, a single piece of film was used and was positioned in the center of the block. Dose distributions can be measured in all three primary anatomical planes (axial, coronal, and sagittal) by changing the orientation of the film block inside the phantom. Four 4.1 mm diameter Delrin bolts and rods compress the block, securing the film in place (Figure 2.2 (b)). These rods can also act as fiducials, providing physical reference locations that allow for localizing the film within the phantom. Vinci *et al*. (2007) reported that this measurement system facilitated localization of dose distribution of areas commonly delivered via stereotactic radiotherapy within a few tenths of a millimeter.

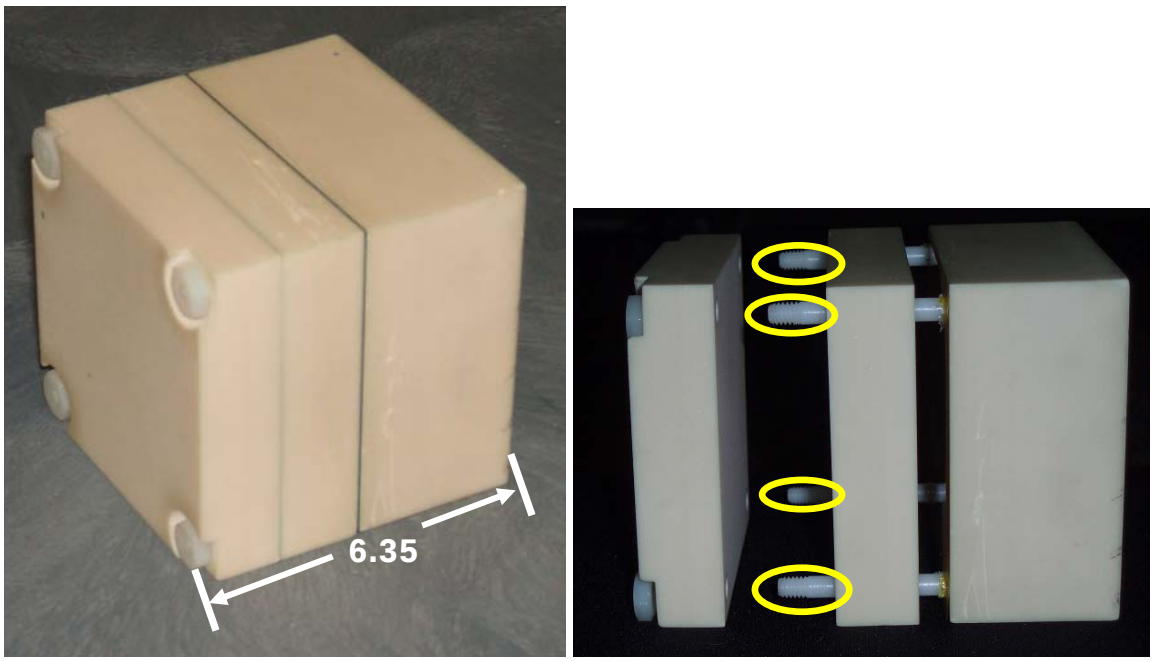

(a) (b)

Figure 2.2 (a) Cubic film block compressed. (b) Film block with Delrin rods circled in yellow.

2.1.2 Phantom CT Scans

CT images of the phantom were acquired using a large bore GE Lightspeed CT Scanner (General Electric Healthcare, Waukesha, WI). During imaging, an S-frame system (Med-Tec,

Orange City, IA) was secured to the CT couch with a head rest (Model F) in place. The phantom was placed on top of the head rest and immobilized using a thermoplastic mask (CIVCO Medical Solutions, Orange City, IA). The phantom was positioned with the axial film plane parallel to the CT imaging plane using two foam boards to achieve proper alignment (Figure 2.3). Achieving proper alignment required scanning the phantom multiple times until the axial film plane was contained within a single CT slice. Once the phantom position was verified, spherical radiopaque markers were placed on the lateral and anterior surfaces of the thermoplastic mask at the laser crosshairs. Doing so allowed for initial positioning of the phantom in the TomoTherapy treatment system.

The current clinically-utilized Mary Bird Perkins Cancer Center (MBPCC) SRS scan protocol was utilized to scan the phantom. However, the field-of-view (FOV) was changed from 30 cm to 50 cm to allow for insertion of the TomoTherapy treatment couch in the TomoTherapy treatment planning system (TPS). The phantom scanning parameters included a slice thickness of 1.25 mm, FOV of 50 cm, matrix size of 512 x 512, 140 kVp voltage, and 380 mA current. A total of three CT scans of the phantom were acquired, one with the film plane in each of the major anatomical planes (axial, coronal, and sagittal).

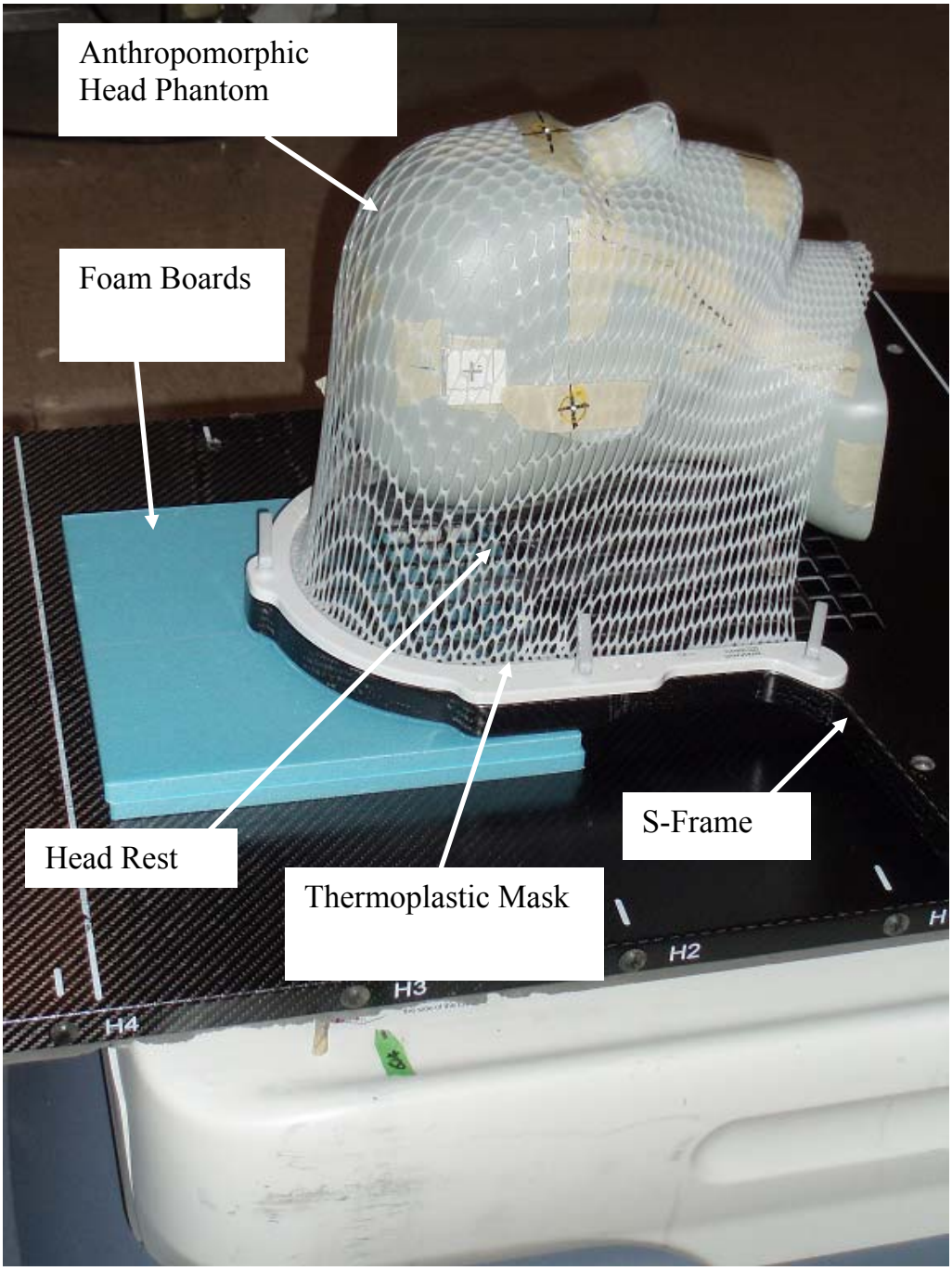

Figure 2.3 Phantom in the scanning position with treatment components labeled.

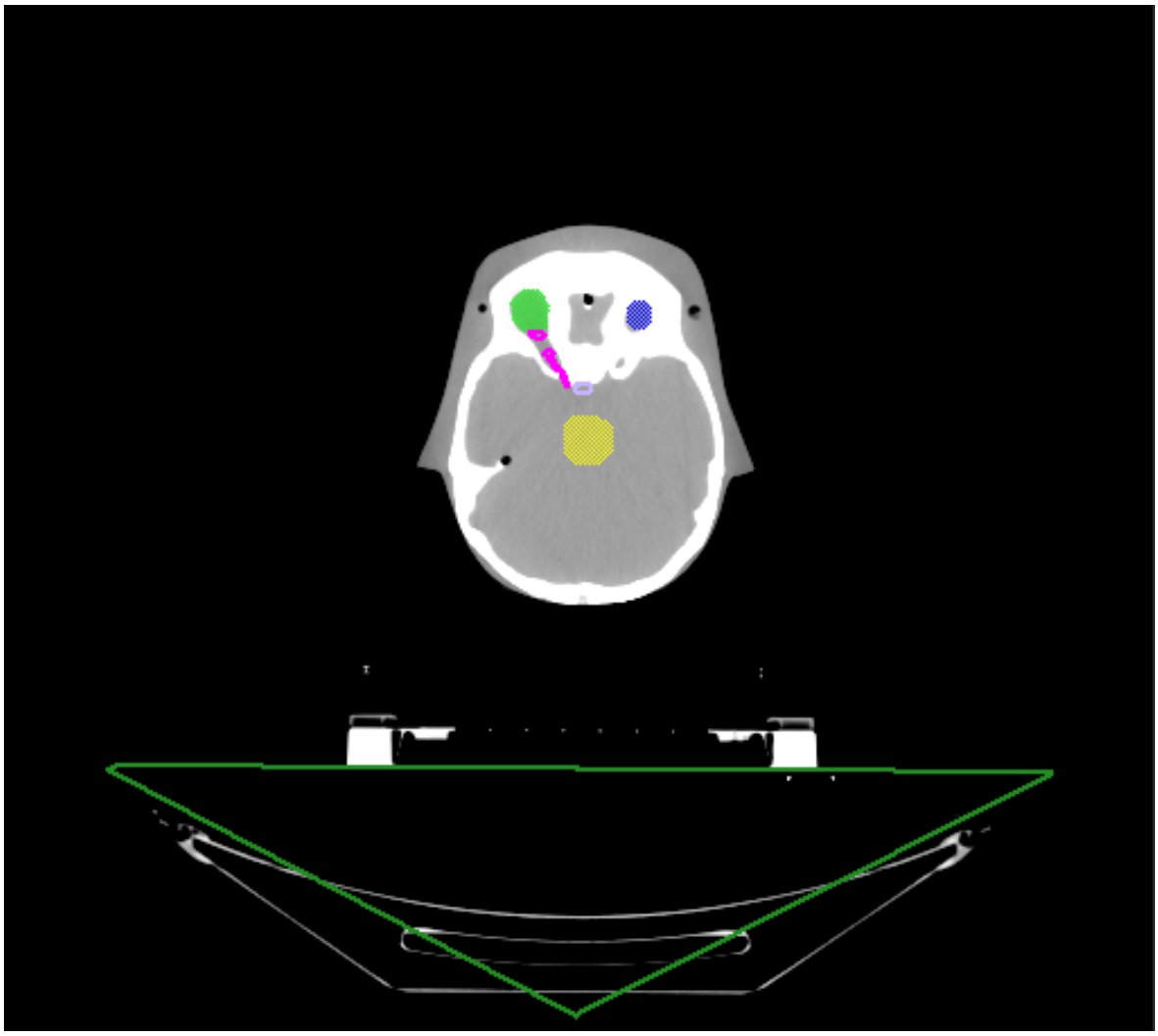

(a)

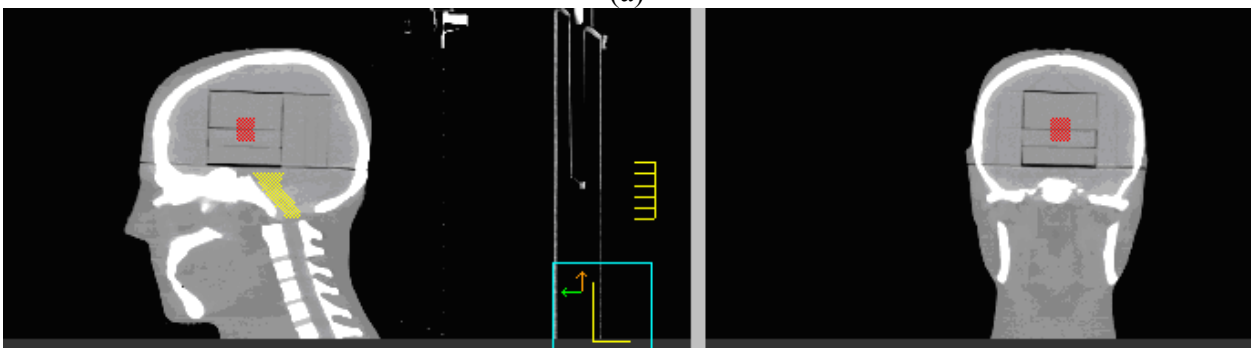

(b) (c)

Figure 2.4 Pinnacle Contours. (a) Axial plane - right and left eye, optic nerve, brain stem and couch. (b) Sagittal plane – PTV and brain stem. (c) Coronal plane – PTV.

2.1.3 Treatment Planning

Each CT series was exported to the Pinnacle treatment planning system (Philips Healthcare, Andover, MA) for contouring. The CT scan with the film orientation in the axial plane was used as the treatment planning CT. A 2-cm diameter x 2-cm long cylindrical PTV was centered within the film block, with the long axis in the superior-inferior direction. This PTV location was selected as a surrogate for a centrally located cranial lesion. Contouring for the brainstem, eyes, optic nerve, optic chiasm, couch, PTV, and a ring (dose –limiting structure) was performed within Pinnacle with the assistance of a MBPCC dosimetrist as needed. Images of the structures contoured in Pinnacle are shown in Figure 2.3. After ROIs were defined, the CT scan and contoured structures were transferred to the TomoTherapy TPS version 3.2.1.

Prior to planning, the CT imaging couch was replaced with the TomoTherapy treatment couch throughout the CT data set. The CT slice where the spherical radiopaque markers were visible and intersected the machine isocenter lasers was determined. Then the in-room setup (red) lasers were manually aligned with the machine isocenter (green) lasers. The PTV was selected as the target, and the remaining structures were ranked in order of avoidance priority (ring, right eye, left eye, brainstem, optic, and optic nerve). The PTV was prescribed a total dose of 120 Gy in 30 fractions to 94% of the volume. This prescription was chosen to allow multiple deliveries of the planned treatment and to place the fraction dose (4 Gy) at the center of the dose range of GafChromic EBT^2 film. A field width of 1.03 cm, a pitch of 0.287, and a fine calculation grid (256 x 256) were set as constraints within the TPS. The ring structure, created in Pinnacle, was used to create a steep fall off of dose outside the PTV by setting constraints on the maximum dose (80.0 Gy) and dose to a specified volume (40 Gy to 45% of the ring). This resulted in a dose gradient of approximately 5%-8% per millimeter outside of the PTV.

After a satisfactory plan was generated, three delivery quality assurance (DQA) plans were created, one with the film plane in each of the principal anatomic planes (axial, coronal, and sagittal). Each CT data set was defined as a DQA phantom in the TomoTherapy treatment planning system. After selecting the appropriate phantom (i.e., desired film plane orientation), the sinogram from the treatment plan was transferred to each of the phantom CT scans and the dose was calculated. A delivery QA procedure was created for each plane so that the fiducial rods were visible in each orientation for registration purposes.

2.2 FILM DOSIMETRY

2.2.1 Film Selection

ISP (International Specialty Products, Wayne, NJ) Gafchromic EBT^2 film was selected for this study due to its large dose range (0 – 800cGy), its insensitivity to visible light, high spatial resolution, minimal energy dependence at 6 MV, near tissue equivalence, and being self-developing. Previous studies have shown the suitability of Gafchromic EBT film for external beam dose verification (Todorovic, Fischer, et al. 2006; Zeidan, Stephenson et al. 2006). Additionally, other types of radiochromic film have been used for SRS dose characterization (McLaughlin, Soares et al. 1994). More recently, radiochromic film was used in a study involving cone beam CT-based stereotactic radiosurgery (Jin, Huh et al. 2009).

2.2.2 Film Preparation

The response of Gafchromic EBT^2 film in scanning is dependent on whether the film is scanned in portrait or landscape orientation (ISP Product Specification Sheet). The differences in response result from anisotropic light scattering because the active component in Gafchromic EBT^2 film is in the form of needle-like particles approximately 1-2 μm in diameter and 15 – 25

μm in length (EBT^2 White Paper, p11). The particles tend to align with the long axes parallel to the coating direction scattering light differently in orthogonal directions (EBT^2 White paper, p11). Because of this, the orientation of the film was maintained throughout the measurement process.

A single piece of 8" x 10" Gafchromic EBT^2 film was cut into 3 strips (≈ 6.3 cm x 25.4 cm) using a paper cutter. Each strip was then cut into smaller pieces (≈ 6.3cm x 6.3cm) using the paper cutter. Each film was marked in the upper right hand corner to maintain the same orientation for all films. After cutting, each film was prepared for use in the phantom using a custom, in-house aluminum film cutting template developed by Vinci *et al*. (2007) (Figure 2.5). Each film was loaded into the template and compressed using two screws to hold the film in place. Holes were drilled in the film using the template's machined holes as a guide so the holes in the film would correspond to the placement of the four fiducial rods of the film cassette. All films were placed in the cutting template in the same orientation for consistency.

(a) (b) (c)

Figure 2.5 (a) Film with orientation marking before drilling. (b) Drilling holes for fiducial rods. (c) Film ready for insertion in Phantom.

2.3 PHANTOM IRRADIATION

2.3.1 Initial Phantom Setup

Prior to each film measurement, a piece of unexposed piece of Gafchromic EBT^2 film was placed inside the film block. For each irradiation, the film was placed with its orientation mark to the right of the arrow on the film block (Figure 2.6). The film insert was then inserted into the phantom head cap. Figure 2.7 shows the orientation of the film insert, and thus the film itself, relative to the phantom anatomy for each of the measurement planes. After inserting the film block in the head cap with the film in the correct anatomical plane for measurement, the phantom was assembled and taped along the seam to ensure the pieces did not separate.

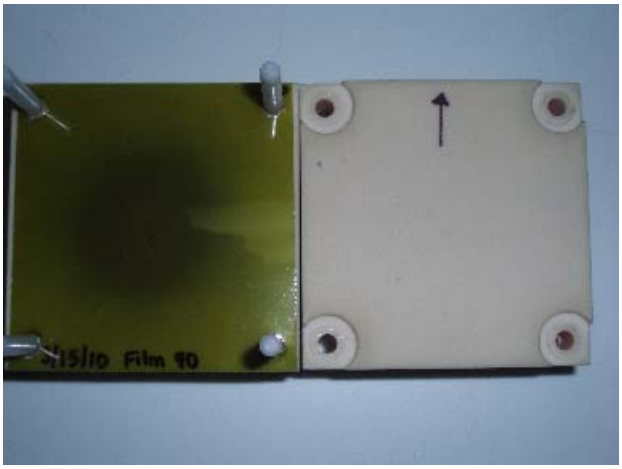

Figure 2.6 Orientation of film in film block. The black mark denoting the film orientation can be seen in the upper right corner.

The phantom was set up on the TomoTherapy treatment couch using the same positioning and immobilization system used for CT scanning. The phantom was positioned such that the radiopaque markers on the lateral and anterior aspects of the immobilization mask coincided with the in-room setup lasers. Additionally, two slabs of plastic water (5 cm thickness) were placed on the bottom portion of the S-frame system to ensure that it did not shift during scanning or treatment.

(a) (b) (c)

Figure 2.7 (a) Axial film block orientation in head cap. The film block was inserted in the phantom head cap such that the arrow on the film block faced the split of the phantom and pointed towards the anterior of the phantom head. (b) Coronal film block orientation in head cap. The film block was inserted in the phantom head cap such that the arrow was facing the anterior of the phantom head and pointed towards the split in the phantom. (c) Sagittal film block orientation in head cap. The film block was inserted in the phantom head cap such that the arrow was facing patient left and pointed towards the split in the phantom head. The position of the film inside the phantom had to be known for registration of the film with the measured dose distribution.

An MVCT scan was acquired using a fine slice thickness of 2mm. The MVCT was automatically registered, using the bony anatomy technique, with the treatment planning CT to determine the necessary shifts to align the phantom to isocenter. The resulting shifts were applied, and the resulting position was considered the nominal position of the phantom.

(a) (b)

Figure 2.8 Misalignment ruler system. (a) Lateral and AP rulers. (b) Vertical ruler.

2.3.2 Sample Space

To determine the IGRT delivery accuracy as a function of initial position, a series of offsets were applied to the position of the phantom. Intentional misalignments of ± 5 mm in the lateral, longitudinal, and vertical directions were applied. Once the phantom was in the nominal position, rulers on the couch top and the machine isocenter lasers were used to determine the offset (Figure 2.8). Shifts were determined by moving the couch in each direction until the intersection of the lasers and rulers showed that the correct offset distance had been reached.

The couch was first offset in the lateral direction using manual couch adjustment knobs at both the head and foot of the couch. The vertical offset was applied using the motorized TomoTherapy couch. Longitudinal offsets were applied by manually moving the couch. Doses were measured in each of the three anatomic planes for nine measurement points: the nominal position with no offset and eight offset points that formed the vertices of a cube about the nominal position. Table 2.1 lists the displacements of each point from the nominal position. Figure 2.9 shows the relative positions of the offset points relative to the nominal position.

Table 2.1 Sample Space Points (distance from nominal position in mm)

Point	Lateral (Right-Left)	Longitudinal (Inferior-Superior)	Vertical (Anterior-Posterior)
0	0	0	0
1	5	5	-5
2	5	-5	5
3	5	-5	-5
4	5	5	5
5	-5	5	5
6	-5	-5	-5
7	-5	-5	5
8	-5	5	-5

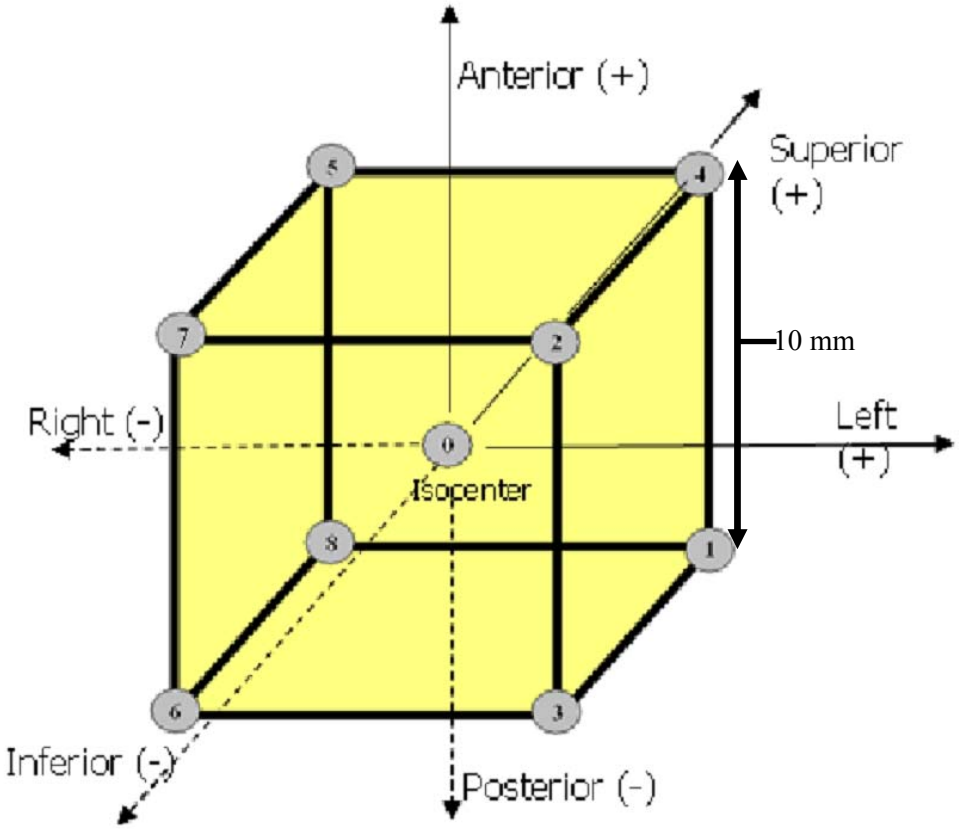

Figure 2.9 Cube defined by intentional misalignments by translations in the lateral, longitudinal, and vertical directions (Vinci 2007). The zero point is isocenter.

2.3.3 Phantom Dose Delivery

Once the appropriate offsets were applied, a volume of slices covering the full phantom was selected, and a fine (2 mm slice thickness) MVCT was acquired. The MVCT was registered to the planning CT using the bony registration algorithm which utilized only those voxels with a value above 1.1 g/cm^3. The registration was visually evaluated using a checkerboard system to view both the TomoTherapy MVCT and planning kVCT (Figure 2.10). This was strictly a qualitative evaluation and no changes were made to the automatic registration results.

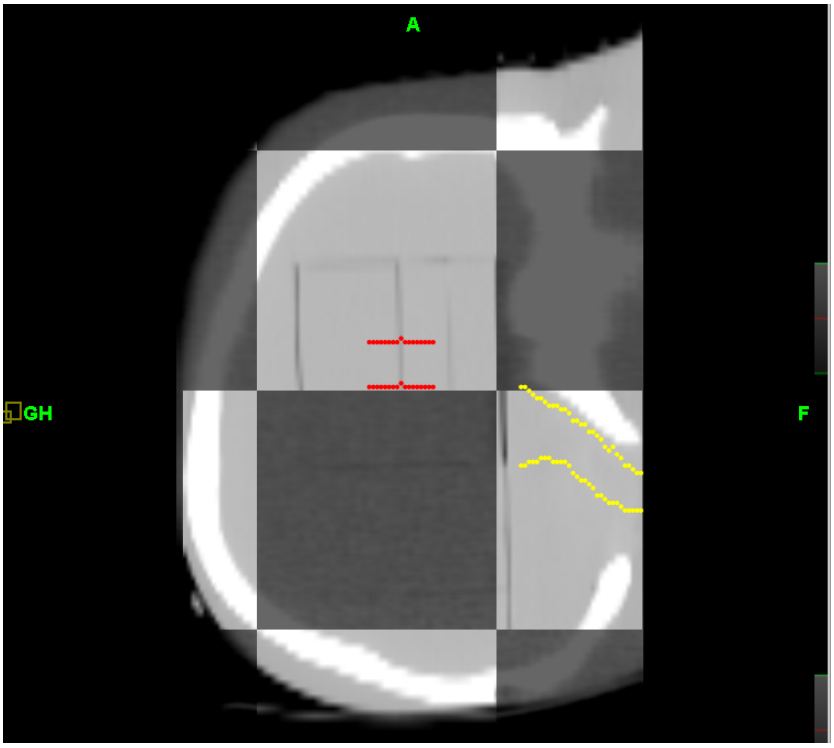

Figure 2.10 MVCT image. Overlay of the MVCT with the planning kVCT; the dark grey is the MVCT and the light grey is the planning kVCT.

The shifts required to position the phantom at the correct location were determined from the registration and applied to the phantom. The vertical and longitudinal shifts were applied automatically while the lateral adjustments were applied manually using the adjustment knobs located at the head and foot of the TomoTherapy treatment couch. Once shifted, the treatment

plan was delivered to the phantom. This procedure was repeated for each sample space point with the film block in each of the three orientations. After treatment, the film was removed, placed in its packaging box, and stored in a light-proof container to allow for self-development overnight.

Four sets of measurements were taken, each set on a separate date (3/10/2010, 3/11/2010, 3/15/2010, and 3/16/2010). For each set, measurements were taken with the phantom's misalignment set to a subset of the sample space points. Offset points were chosen to test each sample space point at least twice with the film block in each of the 3 film plane orientations for each point. During the first set of measurements, points 4, 6, 7, 1, and 5 were tested. The second set of measurements repeated the first set in reverse order. The third set consisted of measurement points 3, 2, 8, and 0, and the fourth set repeated the third in reverse order.

2.4 DATA ANALYSIS

2.4.1 Film Digitization

A template developed by Vinci *et al.* (2008) was used to hold the experimental film for readout. The template consisted of a 14" x 17" blank piece of Kodak (Rochester, NY) EDR2 film into which the experimental films were inserted as shown in Figure 2.11. The films were digitized with a resolution of 0.178 mm using a Vidar (Herndon, VA) DosimetryPRO Advantage(Red) 16-bit film scanner. All films (background, calibration, and experimental) were scanned against the left edge of the slot due to nonuniformities in scanner response across the scanning bed.

RIT113 (Radiological Imaging Technology Inc., Colorado Springs, CO) (v5.2) film dosimetry software was used for all data analysis. A region of interest (ROI) was created that

enclosed each individual test film, and each film was saved as a unique file with an embedded calibration file.

2.4.2 Film Calibration

An 8-field step-and-shoot MLC leaf sequence calibration procedure, similar to that of Childress *et al*. (2002), was used to create calibration films. Calibration films (3/10/2010 & 3/15/2010) were delivered using the 6 MV beam of a Varian (Varian Medical Systems, Palo Alto, CA) 21EX radiotherapy accelerator and a sample calibration film is shown in Figure 2.12(a). A single piece of Gafchromic EBT^2 film was placed in plastic water at 100 cm source-to-axis distance (SAD) at a depth of 10 cm with 5 cm of backscatter. A predefined multileaf collimator sequence was used to create two columns of four 3 x 3 cm^2 dose regions. The absolute dose at the center of each of the eight dose regions and at the center of the film, which received only scatter radiation, was determined using a Model A1SL Exradin miniature Shonka thimble ion chamber using the technique of Childress *et al*. Dose regions 0 – 8 received doses of 11.5, 67.3, 137.8, 199.8, 259.2, 320.4, 392.6, 453.8, and 511.9 cGy, respectively (Figure 2.12(a)).

Each calibration film was scanned as a RIT image file (file extenstion *.rv4) using the Vidar digitizer and RIT software. The low dose column of the calibration curve was scanned first against the left edge of the Vidar scanner, and then the film was rotated 180° and the high dose column was scanned. Since both scans were done in portrait orientation there was no issue in the change of the film response due to the orientation issues previously described a region of interest (ROI) was designated at the center of each dose box and in a region in the center of the calibration film that received only scatter dose. A ROI was created on the unirradiated

background film to obtain a zero dose point. For each ROI, the delivered dose was correlated with the raw analog-to-digital (A/D) value as measured by the Vidar scanner to generate a dose calibration curve to be applied to the experimental films (Figure 2.12). A 5 pixel x 5 pixel median filter was applied to each image for isolated noise and artifact reduction. A piecewise polynomial was applied to the measured data in the RIT software and used as the dose calibration curve.

(a) (b)

Figure 2.11: (a) Film scanning template. (b) Film being scanned.

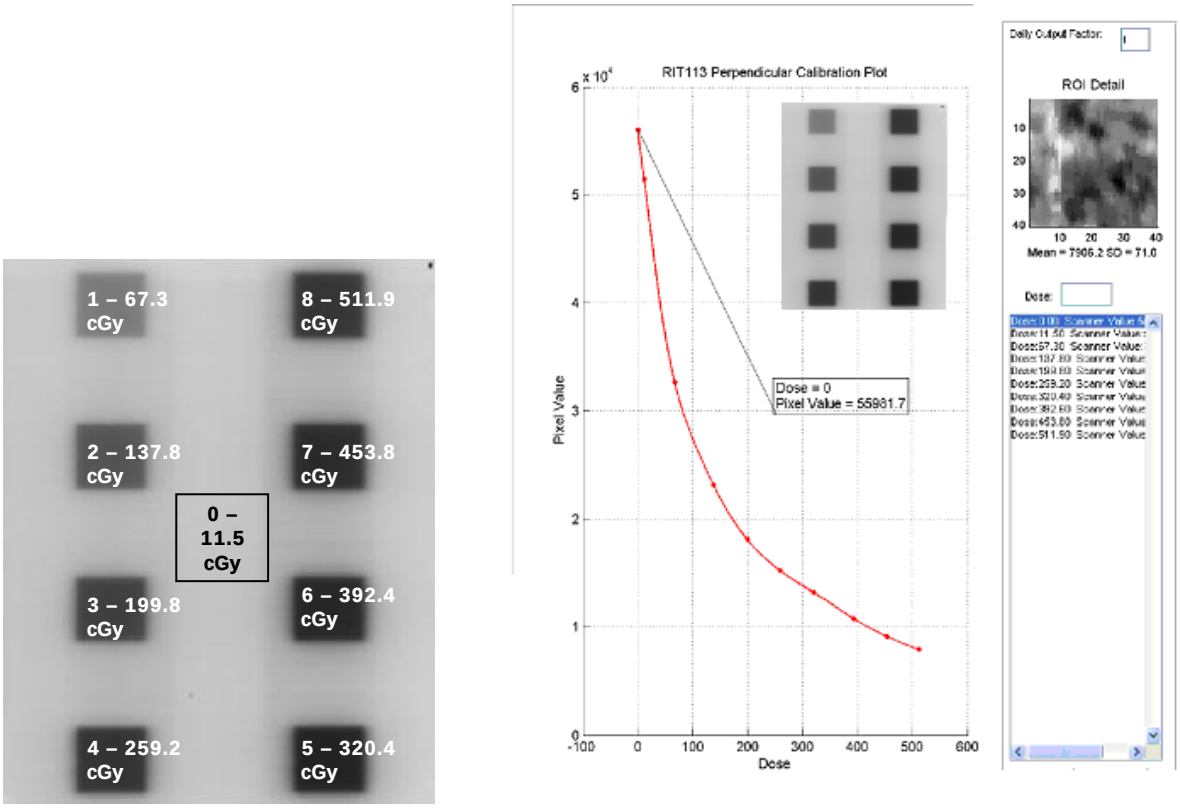

(a) (b)

Figure 2.12. (a) Calibration film labeled with doses. (b) Gafchromic EBT^2 dose calibration curve from RIT.

2.4.3 Planar Dose Export

Within the TomoTherapy TPS, there is an "extract dose plane" feature in the DQA Analysis that allows the user to extract a single 2D dose plane from the 3D dose matrix. To use this feature, a test film was read into the DQA Analysis along with a calibration film file used to convert the experimental film values to absolute dose. Once the test film was converted to dose it was registered to its corresponding location in the phantom CT data set. For registration, the general axial, general coronal, or general sagittal method was selected depending on which dose plane was being extracted. The general registration method allows the user to select two points on the film and select the corresponding points on the phantom for registration. Using the

selected registration method, two points (opposite fiducial rods) on the film and corresponding plane in the CT data set were selected for registration (Figure 2.13).

The coordinates of the registration points (i.e., fiducial rods) in the treatment planning CT scan were determined for each of the three principal planes. This was done by selecting the plane that corresponded to the film plane and manually determining the center of each fiducial rod. The location of the film plane was selected by identifying the plane where the two halves of the dosimetry insert joined together. The coordinates of the centers of the fiducial rods from the center of the image were determined using the readout feature in the TomoTherapy TPS which gives the coordinates in terms of the machine isocenter. To determine the coordinates for the fiducial rods, the image was magnified and then the cursor was placed in the center of each of the rods and the coordinates were recorded. This process was performed for each DQA CT data set, one for each film plane orientation.

For the axial film block orientation, the machine isocenter is the same as the image center, but for the coronal and sagittal film block orientation this is not the case. The CT images for the coronal and sagittal film block orientations had 112 slices in the superior - inferior direction; the acquisition was zeroed at the spherical radiopaque marker location on the thermoplastic mask, not the machine isocenter. The center of the image for both the coronal and sagittal film block orientation was shifted 3.0 cm superiorly from the machine isocenter. This shift was taken into account when recording the coordinates of the 4 fiducial rods for both the coronal and sagittal film block orientation. Also, when performing TomoTherapy Delivery QA (DQA) Analysis, there is a systematic shift between the planning and DQA coordinate systems in both the anterior-posterior direction and the left-right direction of 0.2 cm. This shift was also accounted for when recording the coordinates of the 4 fiducial rods for the registration templates.

After registration of the film and corresponding CT plane was complete, the "extract dose plane" feature was used to export the planar dose at the location in the dose matrix. The axial dose grid size was a 256 x 256 matrix, and the coronal and sagittal dose grid size was a 112 x 256 matrix. The spatial resolution of the dose grid for each scan was 1.95 mm due to the larger FOV (50 cm). Planar dose distributions were created for each of the three principal planes.

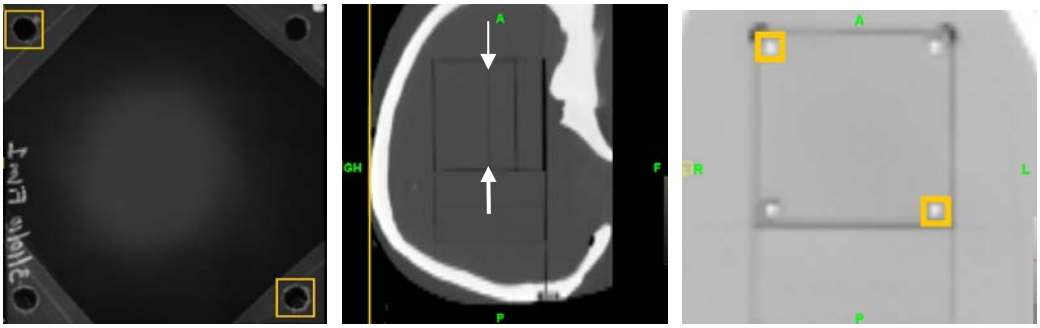

(a) (b) (c)

Figure 2.13 Demonstration of registration of film to planar dose in TomoTherapy TPS using the general axial method. (a) Two points on film selected. (b) Film plane selected (film plane is designated using the arrows). (c) Selection of the corresponding points for registration on the phantom.

2.4.4 Registration of Film and Planar Doses

To register the measured dose distributions with the TomoTherapy calculated dose distributions, registration templates were created in RIT with the coordinates for the fiducial rods in each of the principal planes. The templates were created by entering the coordinates of the fiducial rods in terms of the center of the image for each plane orientation. The appropriate template (axial, coronal, or sagittal) was then applied to the TomoTherapy extracted planar dose.

A region surrounding the hole on the digitized film image (corresponding to a fiducial rod) was selected. In a magnified view, the cursor was manually positioned at the center of the fiducial rod hole that corresponded to the appropriate fiducial rod location in the planar dose, and the registration point was positioned. This process was repeated for the remaining three holes on

the film image. Once each of the registration points was placed at the center of the hole, the film image was registered to the corresponding planar dose using a point based rigid body registration technique. The manual registration technique is shown in Figure 2.14.

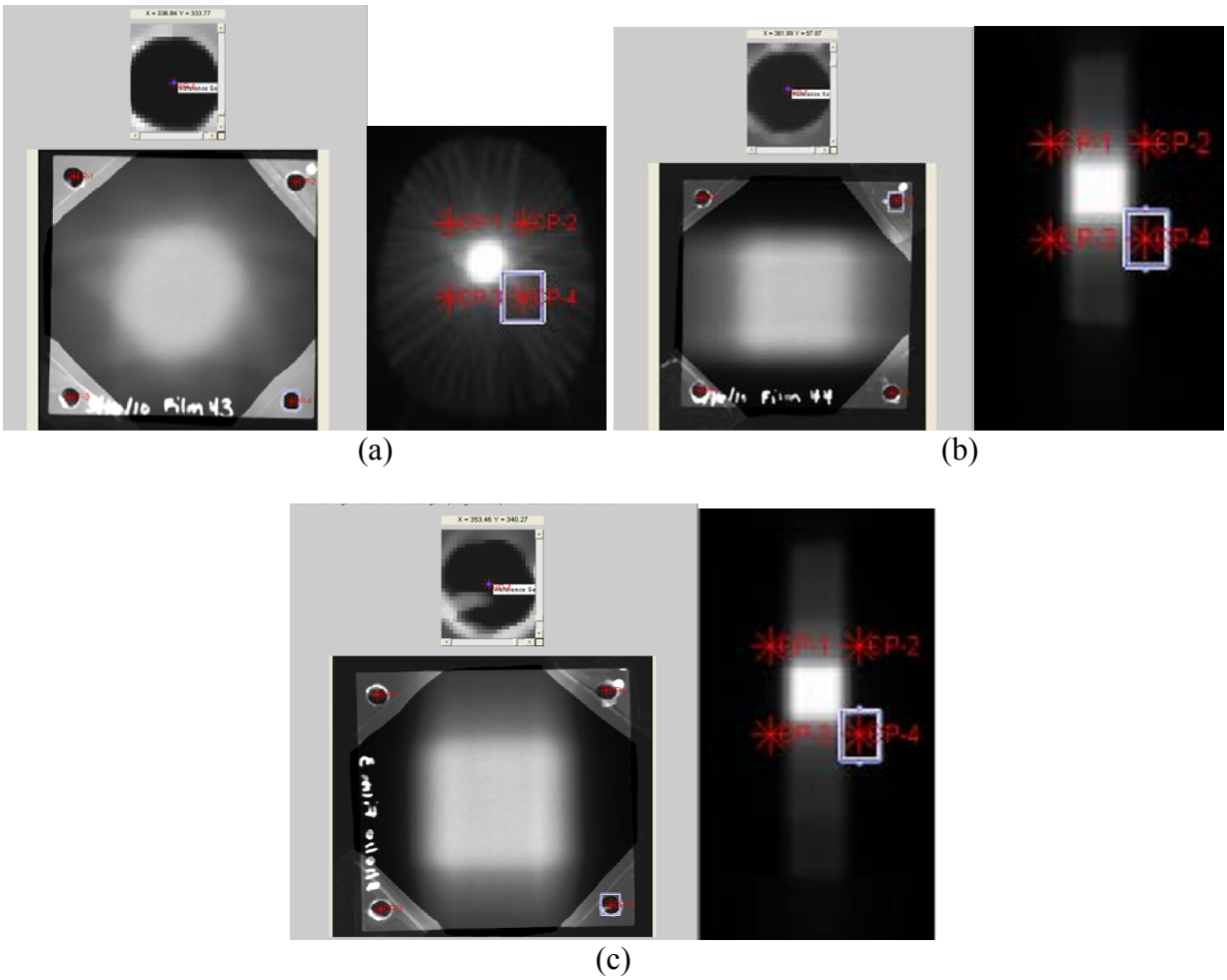

Figure 2.14. Manual registration of measured and calculated dose distributions for (a) axial film plane (b) coronal film plane (c) sagittal film plane.

2.4.5 Analysis Metrics

Differences between the planned and delivered dose distributions were quantified by taking film profiles along the vertical and horizontal axes (Figure 2.15). In all cases, the dose distributions were normalized to 100% in the center of the PTV. The analysis metrics used here

were previously defined by Vinci *et al.* (2008). The analysis metrics evaluate both the position and shape of the measured distribution compared to the calculated distribution.

The positional alignment error (Δc) is the displacement between the midpoints of the calculated and measured profiles at the 70% dose level. The

$$\Delta c = \tfrac{1}{2}(70\%_{\text{film 2}} + 70\%_{\text{ film 1}}) - \tfrac{1}{2}(70\%_{\text{TPS2}} + 70\%_{\text{TPS 1}}). \quad (1)$$

where 70% refers to the position of the 70% dose point and subscripts 1 and 2 refer to the positive slope of the profile and negative slope of the profile while moving across the profile from left to right (see Figure 2.16). The 70% dose level was selected because it is close to the location of the steepest dose gradient. The Δc metric is a measure of the alignment error in a particular measurement.

Comparison of shifts in the 80% dose points (Δ80) has greater relevance for the basis of clinical decisions as it represents the minimum acceptable dose coverage in SRS procedures. 80% dose point shifts were defined as follows:

$$\Delta 80_{\text{Anterior}} = 80\%_{\text{TPS,A}} - 80\%_{\text{film,A}} \quad (2)$$

$$\Delta 80_{\text{Posterior}} = 80\%_{\text{film,P}} - 80\%_{\text{TPS,P}} \quad (3)$$

$$\Delta 80_{\text{Right}} = 80\%_{\text{TPS,R}} - 80\%_{\text{film,R}} \quad (4)$$

$$\Delta 80_{\text{Left}} = 80\%_{\text{film,L}} - 80\%_{\text{TPS,L}} \quad (5)$$

$$\Delta 80_{\text{Superior}} = 80\%_{\text{TPS,S}} - 80\%_{\text{film,S}} \quad (6)$$

$$\Delta 80_{\text{Inferior}} = 80\%_{\text{film,I}} - 80\%_{\text{TPS,I}} \quad (7)$$

The subscripts A, P, S, I, L, and R denote the anterior, posterior, superior, inferior, left, and right sides of the profile, respectively. The subscripts film and TPS denote whether the reported 80% value was obtained from the film profile or planning system profile, respectively. Positive values

of Δ80 indicated that the measured 80% isodose line was outside the calculated (planned) 80% isodose line. Conversely, negative values of Δ80 indicated that the measured 80% isodose line was inside the calculated (planned) 80% isodose line. (see Figure 2.17).

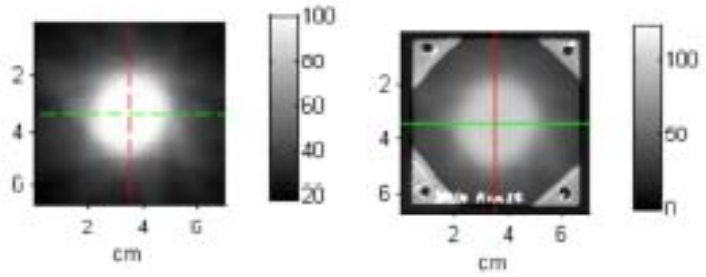

(a) (b)

Figure 2.15. Horizontal (green) and vertical (red) profiles for the (a) calculated and (b) measured dose distributions.

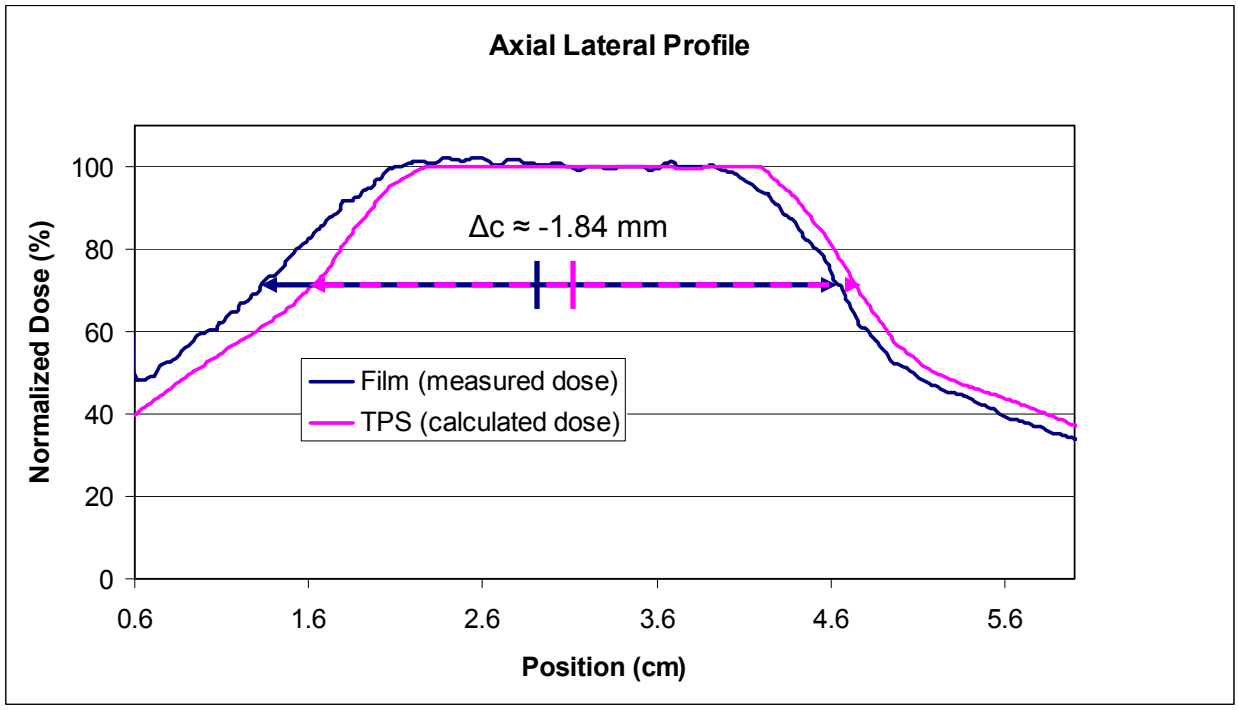

Figure 2.16 Demonstration of the Δc metric

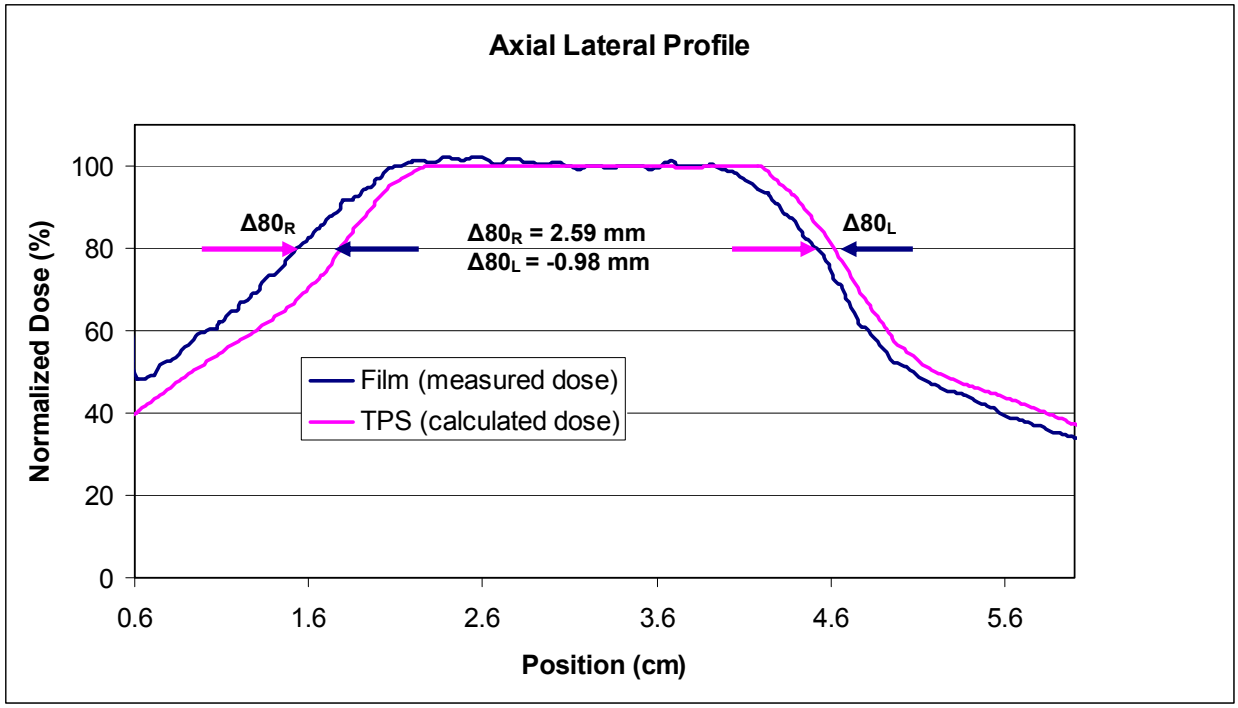

Figure 2.17 Demonstration of the Δ80 metric.

2.4.6 Uncertainty in Analysis Metrics

To determine the uncertainty in the analysis metrics from the registration and analysis process, the same film was registered to itself ten times, and the quantities used for analysis were determined for each registration. Ideally, since identical distributions are being registered, all of the metrics should have means and standard deviations of zero. Deviations from zero indicate the errors introduced in the manual registration of the data sets and the calculation of the metrics used to analyze the data.

To determine the uncertainty introduced by the use of the calculated planar dose distributions, the same film was registered 10 times to its corresponding TPS dose distribution. This was done for a film in each of the three principal planes, and the quantities used for analysis were determined for each registration. Since differences are expected between the calculated and

measured distributions, the mean value of each quantity can not be expected to be zero. For this analysis, the standard deviations of the metrics was calculated and used as the minimum uncertainty achievable in the analysis process.

2.5 REFERENCES

ISP Products."Gafchromic EBT^2 Film Self-Developing Film for Radiotherapy Dosimetry."EBT2 White Paper. 3 March 2009. http://online.ispcorp.com/_layouts/Gafchromic/index.html .

Holmes, T. W., R. Hudes, et al. (2008). "Stereotactic Image-Guided Intensity Modulated Radiotherapy Using the Hi-Art II Helical Tomotherapy System." Medical Dosimetry **33**(2): 135 – 148.

Jin, H., S. Huh, et al. (2009). " Dosimetric Verification of Ultra Small Fields of Image-Guided Linac-Based Stereotactic Radiosurgery." Medical Physics 36(abstract): 2430.

McLaughlin, W.L., C.G. Soares, et al. (1994). " The use of Radiochromic Detector for the Determination of Stereotactic Radiosurgery Dose Characteristics." Medical Physics **21**(3): 379 – 388.

Soisson, E. T., G. Sobering, et al. (2009). "Quality Assurance Of An Image Guided Intracranial Stereotactic Positioning System." Technology in Cancer Research and Treatment **8**(1):39 – 49.

Vinci, J. (2007). Accuracy of Cranial Coplanar Beam Therapy with BrainLab Exactrac Image Guidance. Physics and Astronomy. Baton Rouge Louisiana State University and Agricultural and Mechanical College. **Master of Science**: 139.

Vinci, J.P., K. R. Hogstrom, et al. (2008). "Accuracy of Cranial Coplanar Beam Therapy Using an Oblique, Stereoscopic X-Ray Image Guidance System." Medical Physics **35**(8): 3809 – 3819.

Zeidan, O. A., S.A.L. Stephenson, et al. (2006). "Characterization and use of EBT Radiochromic Film for IMRT Dose Verification." Medical Physics **33**(11): 4064 – 4072.

CHAPTER 3: RESULTS AND DISCUSSION

3.1 UNCERTAINTY IN ANALYSIS METRICS

Table 3.1 shows the results of registering a single film to itself ten times and evaluating the comparison metrics as previously described. Ideally, all of the metrics would have a value of 0.00 mm since the compared dose distributions are identical. The values for all of the metrics are less than the film pixel resolution of 0.178 mm. This indicates than the manual registration technique and extraction of the analysis metrics is limited by the pixel resolution of the film.

Table 3.1 Results from registering the same film to itself 10 times.

Metric	Mean ± Standard Deviation
$\Delta 80_A$	-0.02 mm ± 0.01 mm
$\Delta 80_P$	0.01 mm ± 0.01 mm
Δc_{A-P}	0.00 mm ± 0.01 mm
$\Delta 80_R$	-0.02 mm ± 0.01 mm
$\Delta 80_L$	0.05 mm ± 0.02 mm
Δc_{R-L}	-0.02 mm ± 0.01 mm

The results of multiple registrations of the same film to a single TomoTherapy planar dose to determine uncertainties resulting from registering a film to a planar dose distribution are shown in Table 3.2. These results present the standard deviation of the specified metric over the ten registrations. The results are comparable to the results of Table 1 (film–to-film registration) indicating that the registration of a film and planar dose are again limited by the pixel resolution of the film (0.178 mm) and not the manual selection of the registration points.

Table 3.2 Results from registering the same film 10 times with its corresponding planar dose (calculated dose). SD = standard deviation

Film 43 – Axial	**Film 44 – Coronal**	**Film 45 – Sagittal**
$\Delta 80_A$ SD = 0.03 mm	$\Delta 80_I$ SD = 0.02 mm	$\Delta 80_S$ SD = 0.04 mm
$\Delta 80_P$ SD = 0.04 mm	$\Delta 80_S$ SD = 0.02 mm	$\Delta 80_I$ SD = 0.04 mm
Δc_{A-P} SD = 0.02 mm	Δc_{I-S} SD = 0.01 mm	Δc_{S-I} SD = 0.02 mm
$\Delta 80_R$ SD = 0.03 mm	$\Delta 80_L$ SD = 0.03 mm	$\Delta 80_P$ SD = 0.06 mm
$\Delta 80_L$ SD = 0.02 mm	$\Delta 80_R$ SD = 0.02 mm	$\Delta 80_A$ SD = 0.04 mm
Δc_{R-L} SD = 0.02 mm	Δc_{L-R} SD = 0.01 mm	Δc_{P-A} SD = 0.01 mm

3.2 RESULTS OF PHANTOM IRRADIATIONS

Phantom doses were delivered over four sessions (3/10/2010, 3/11/2010, 3/15/2010, & 3/16/2010). Table 3.3 shows the results for all treatments delivered. A negative Δc indicates a shift of the measured profile in the right, anterior, or superior direction relative to the calculated profile. Negative values of Δ80 indicated that the measured 80% isodose line was inside the calculated (planned) 80% isodose line while positive values of Δ80 indicated that the measured 80% isodose line was outside the calculated (planned) 80% isodose line.

A summary of the results for the analsysis metrics are shown in Figure 3.1 and Figure 3.2. All quantities are presented in millimeters. The differences (mean ± standard deviation) in Δc (Figure 3.1) were -0.15 ± 0.47 mm (range: -1.97 to 0.8 mm; μ_σ (standard error of the mean, N = 36) = 0.08 mm), -0.36 ± 0.56 mm (range: -1.25 to 0.63 mm; μ_σ = 0.09 mm), and -0.67 ± 0.93 mm (range: -3.04 to 0.90 mm, μ_σ = 0.16 mm) in the superior-inferior, anterior-posterior, and lateral directions, respectively.

Table 3.3(a) Metrics for measurement Sets 1 and 2. All data are given in millimeters.

Measurement Set 1		Axial Film Plane						Coronal Film Plane						Sagittal Film Plane					
Sample Space Point	Offset Coordinates	$\Delta 80_R$	$\Delta 80_L$	$\Delta 80_A$	$\Delta 80_P$	Δc_{RL}	Δc_{AP}	$\Delta 80_L$	$\Delta 80_R$	$\Delta 80_I$	$\Delta 80_S$	Δc_{RL}	Δc_{SI}	$\Delta 80_P$	$\Delta 80_A$	$\Delta 80_S$	$\Delta 80_I$	Δc_{AP}	Δc_{SI}
4	(5,5,5)	2.59	-0.98	0.79	-0.01	-1.84	-0.52	-1.38	2.48	0.65	0.29	-1.84	0.12	0.63	0.22	0.27	0.56	0.09	0.20
6	(-5,-5,-5)	0.46	0.75	0.87	-0.33	0.34	-0.57	-0.06	0.85	-0.16	1.09	-0.35	-0.65	-0.34	0.77	0.62	0.42	-0.66	-0.06
7	(-5,-5,5)	-0.05	1.53	0.68	-0.04	0.76	-0.25	0.28	0.43	1.18	-0.26	-0.01	-0.60	0.58	-0.03	0.74	0.09	0.29	-0.35
1	(5,5,-5)	1.05	-0.02	1.53	-1.00	-0.52	-1.25	0.17	1.45	-0.23	0.98	-0.57	0.80	-0.56	0.76	2.39	-1.57	-0.66	-1.97
5	(-5,5,5)	0.47	1.03	0.73	0.21	0.27	-0.15	0.69	0.31	1.11	0.07	0.17	0.45	1.25	-0.35	-0.07	0.94	0.87	0.42

Measurement Set 2		Axial Film Plane						Coronal Film Plane						Sagittal Film Plane					
Sample Space Point	Offset Coordinates	$\Delta 80_R$	$\Delta 80_L$	$\Delta 80_A$	$\Delta 80_P$	Δc_{RL}	Δc_{AP}	$\Delta 80_L$	$\Delta 80_R$	$\Delta 80_I$	$\Delta 80_S$	Δc_{RL}	Δc_{SI}	$\Delta 80_P$	$\Delta 80_A$	$\Delta 80_S$	$\Delta 80_I$	Δc_{AP}	Δc_{SI}
5	(-5,5,5)	0.50	0.73	0.30	-0.02	-0.12	-0.19	0.39	1.15	0.43	0.24	-0.52	0.14	0.61	-0.01	0.52	0.32	0.26	-0.08
1	(5,5,-5)	-0.09	1.72	1.31	-0.69	0.90	-0.78	-1.40	2.970	0.22	0.37	-2.09	-0.04	-0.19	0.58	0.97	0.02	-0.46	-0.49
7	(-5,-5,5)	0.12	1.05	0.35	0.63	0.46	0.21	0.89	0.26	0.14	0.75	0.37	-0.30	0.65	-0.08	0.16	0.23	0.41	0.07
6	(-5,-5,-5)	1.26	1.08	1.49	-0.86	-0.17	-1.15	-0.52	1.62	0.22	0.33	-1.20	-0.11	0.08	0.77	0.98	-0.22	-0.52	-0.53
4	(5,5,5)	0.75	0.62	0.57	-0.43	-0.29	-0.37	-2.24	3.62	0.80	0.54	-3.04	0.07	0.65	0.19	0.44	0.72	0.21	0.05

Table 3.3(b) Metrics for measurement Sets 3 and 4. All data are given in millimeters.

Measurement Set 3		Axial Film Plane						Coronal Film Plane						Sagittal Film Plane					
Sample Space Point	Offset Coordinates	$\Delta 80_R$	$\Delta 80_L$	$\Delta 80_A$	$\Delta 80_P$	Δc_{RL}	Δc_{AP}	$\Delta 80_L$	$\Delta 80_R$	$\Delta 80_I$	$\Delta 80_S$	Δc_{RL}	Δc_{SI}	$\Delta 80_P$	$\Delta 80_A$	$\Delta 80_S$	$\Delta 80_I$	Δc_{AP}	Δc_{SI}
3	(5,-5,-5)	2.06	-0.40	0.95	-0.55	-1.42	-0.96	-0.72	1.98	0.37	0.46	-1.33	-0.04	-0.92	1.55	0.97	0.09	-1.09	-0.51
2	(5,-5,5)	1.75	-0.56	-0.33	0.78	-1.28	0.53	-1.29	2.27	-0.16	0.71	-1.66	-0.36	1.05	-0.040	0.53	0.21	0.63	-0.23
8	(-5,5,-5)	0.27	1.30	1.45	-0.55	0.66	-0.86	0.06	1.22	1.28	-0.07	-0.48	0.63	-0.10	0.41	0.26	0.56	-0.35	0.14
0	(0,0,0)	1.41	-0.27	1.27	-0.79	-0.98	-1.24	-1.47	2.15	0.89	0.61	-1.76	0.22	0.31	0.31	0.70	0.16	-0.15	-0.17

Measurement Set 4		Axial Film Plane						Coronal Film Plane						Sagittal Film Plane					
Sample Space Point	Offset Coordinates	$\Delta 80_R$	$\Delta 80_L$	$\Delta 80_A$	$\Delta 80_P$	Δc_{RL}	Δc_{AP}	$\Delta 80_L$	$\Delta 80_R$	$\Delta 80_I$	$\Delta 80_S$	Δc_{RL}	Δc_{SI}	$\Delta 80_P$	$\Delta 80_A$	$\Delta 80_S$	$\Delta 80_I$	Δc_{AP}	Δc_{SI}
0	(0,0,0)	1.48	-0.04	0.95	-0.42	-0.84	-0.55	-0.63	1.43	-0.03	0.72	-1.10	-0.37	0.350	0.30	0.73	0.41	-0.10	-0.08
8	(-5,5,-5)	1.12	0.66	1.12	-0.26	-0.37	-0.76	0.72	0.10	0.46	0.61	0.36	-0.07	-0.20	0.74	0.38	0.49	-0.60	-0.03
2	(5,-5,5)	1.31	-0.15	0.81	-0.14	-0.92	-0.44	-0.97	2.29	-0.33	1.31	-1.67	-0.69	0.68	0.19	0.58	-0.18	0.16	-0.44
3	(5,-5,-5)	0.98	-0.11	1.23	-1.24	-0.41	-1.20	-1.31	1.91	0.46	0.95	-1.53	-0.24	-0.28	0.76	0.62	0.42	-0.62	-0.21

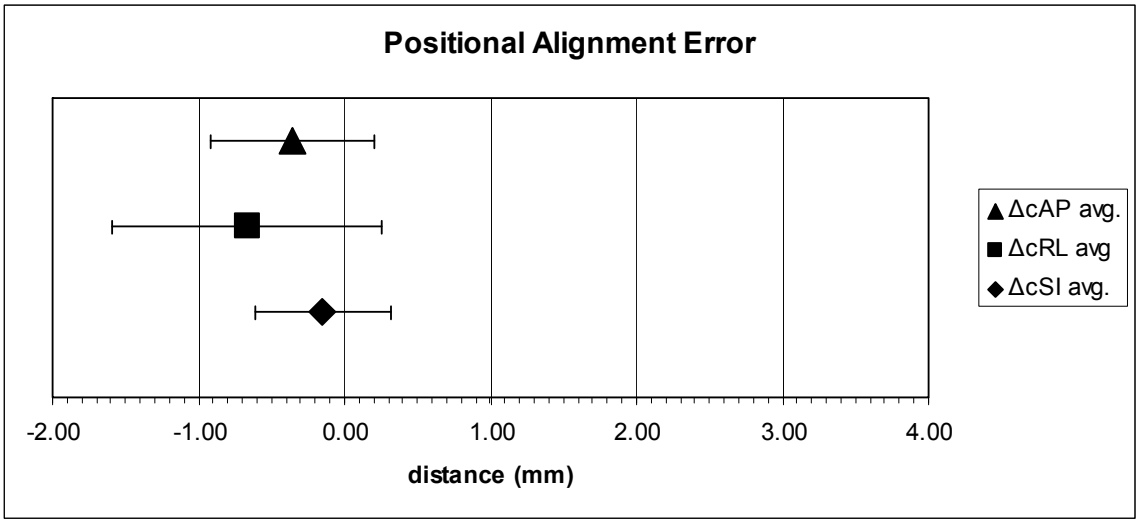

Figure 3.1 Treatment delivery results for analysis quantity Δc. The data point is the mean value and the error bars show a range of ±1 standard deviation.

The standard deviation of the positional alignment error (Δc) is a measure of the reproducibility of alignment with the planning CT using the MVCT image guidance. The reproducibility (2σ) of TomoTherapy MVCT alignment was within 1.86 mm for all directions. The lateral reproducibility was the worst, and is believed to be due to the manual realignment of the phantom in the lateral direction (Section 2.8)). It was noticed that while realigning the phantom, the TomoTherapy readout scale would show couch movement while the rulers in place for misalignment of the phantom did not indicate the couch was moving the same distance as the readout indicated. This effect was not quantitatively measured, but is believed to be due to backlash in the drive screws. Based on the values for $\Delta c \pm \sigma$ and the standard error of the mean, all of the quantities ($\Delta c_{S\text{-}I}$, $\Delta c_{Lateral}$, $\Delta c_{A\text{-}P}$) are statistically significantly different from the expected value of zero.

Figure 3.2 shows the mean and standard deviation for the displacement of the measured 80% dose point and the calculated 80% dose point for each direction. For the four measurement sessions, the mean displacements of the measured 80% dose points in millimeters were 1.28 ±

0.91 (range: -0.09 to 3.62; μ_σ = 0.15 mm, N=36), -0.02 ± 0.96 (range: -2.24 to 1.72; μ_σ = 0.16 mm), -0.04 ± 0.62 (range: -1.24 to 1.25; μ_σ = 0.10 mm), 0.64 ± 0.52 (range: -0.35 to 1.55; μ_σ = 0.09 mm), 0.30 ± 0.52 (range: -1.57 to 1.28; μ_σ = 0.09 mm), and 0.60 ± 0.46 (range: -0.26 to 2.39; μ_σ = 0.08 mm) for the right, left, posterior, anterior, inferior, and superior directions, respectively. Again, the largest mean difference and the largest standard deviations for these metrics occurred in the lateral direction. Again, this is believed to be due to the accuracy and precision on the manual positioning of the couch in the lateral direction compared to the automated couch positioning in the AP and SI directions.

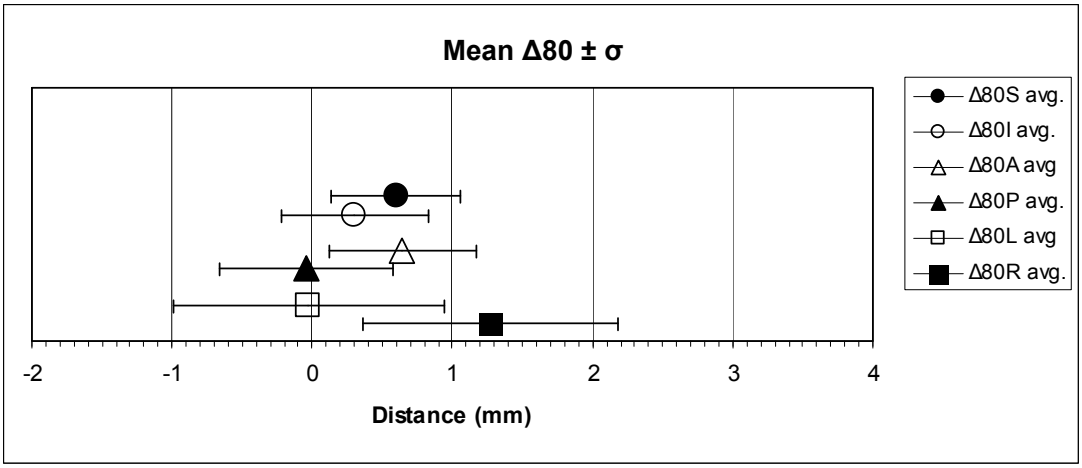

Figure 3.2 Treatment delivery results for analysis quantity Δ80. The standard deviation for each quantity is shown using error bars.

Figure 3.3 shows histograms for all of the data by film plane. Qualitatively it appears the data followed a Gaussian distribution. The histograms were plotted to see the variation between metrics measured in different film planes. The mean $\Delta 80_R$ for the axial film plane was 0.97 ± 0.74 mm and the mean $\Delta 80_R$ for the coronal was 1.58 ± 0.98 mm. The mean $\Delta 80_L$ for the axial was 0.44 ± 0.78mm and the mean for the coronal was -0.49 ± 0.92 mm. For $\Delta 80_A$, the mean and standard deviation in millimeters were determined to be 0.89 ± 0.48 and 0.39 ± 0.45 for the axial and sagittal respectively. The mean and standard deviation in millimeters were determined to be -0.32 ± 0.53 and 0.24 ± 0.58 for $\Delta 80_P$ in the axial and sagittal planes

respectively. The mean and standard deviation for $\Delta 80_S$ were 0.41 ± 0.50 mm and 0.20 ± 0.53 mm for the coronal and sagittal planes respectively. The mean and standard deviation of $\Delta 80_I$ for the coronal and sagittal planes were determined to be 0.54 ± 0.41 mm and 0.66 ± 0.52 mm, respectively. Ideally corresponding values measured in different planes would be exactly the same; however, because the whole process from setup to treatment has to be repeated for each film there is some variation.

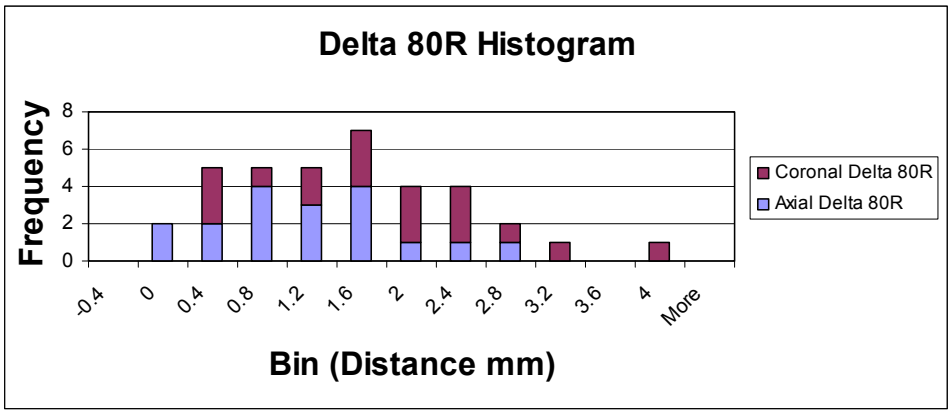

(a)

Figure 3.3(a) Histogram for $\Delta 80_R$ metric.

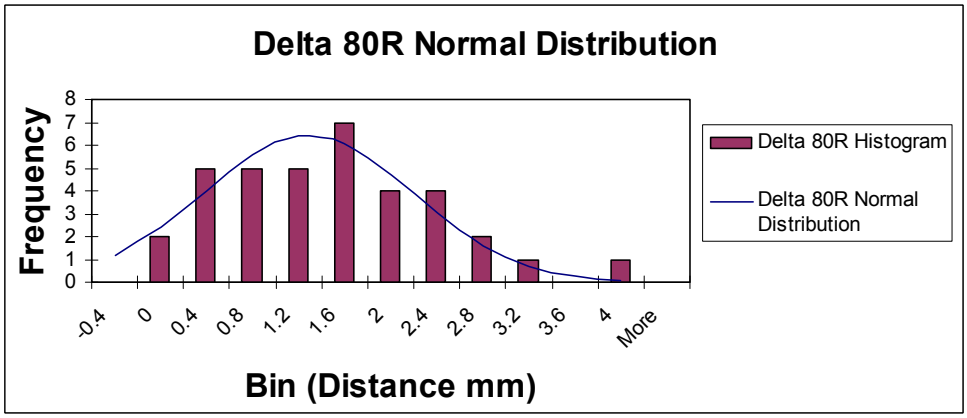

(b)

Figure 3.3(b) Normal distribution for $\Delta 80_R$ metric.

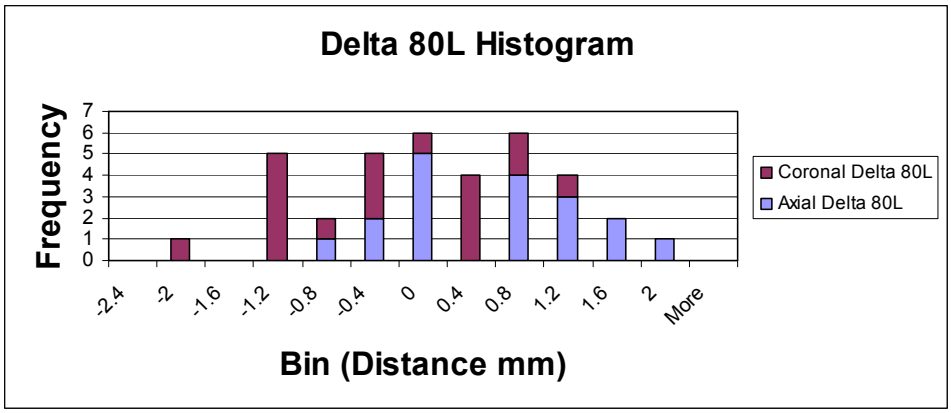

(c)

Figure 3.3(c) Histogram for $\Delta 80_L$ metric.

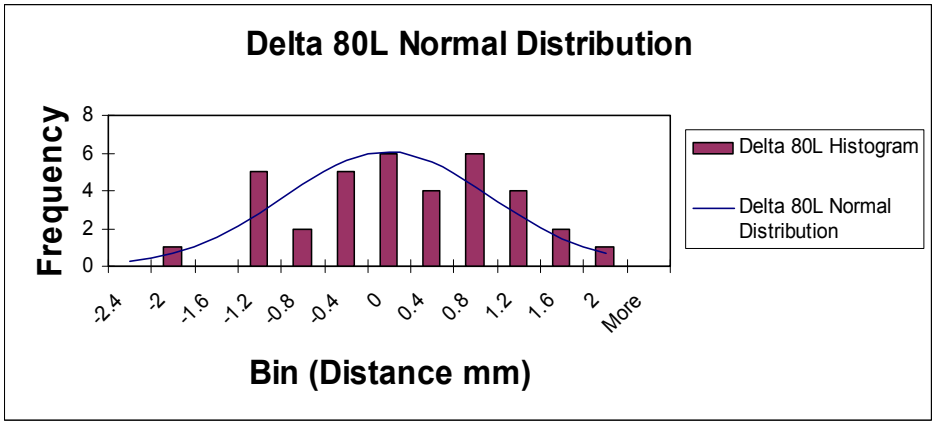

(d)

Figure 3.3(d) Normal distribution for $\Delta 80_L$.

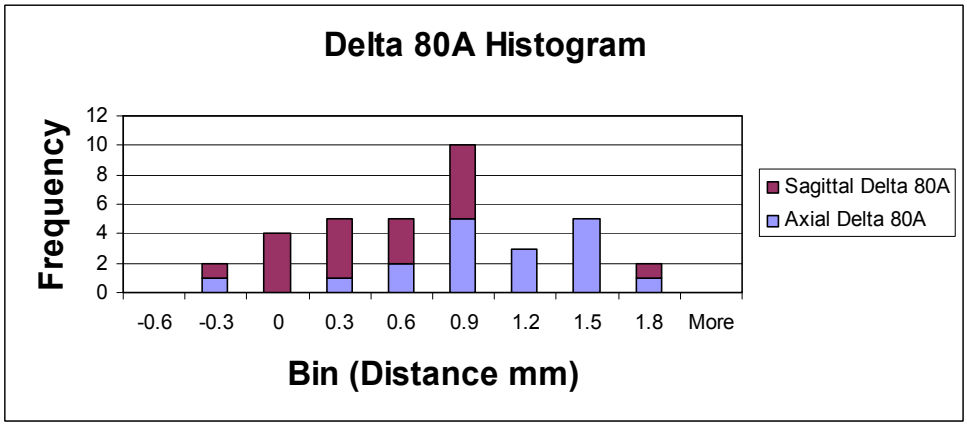

(e)

Figure 3.3(e) Histogram for $\Delta 80_A$ metric.

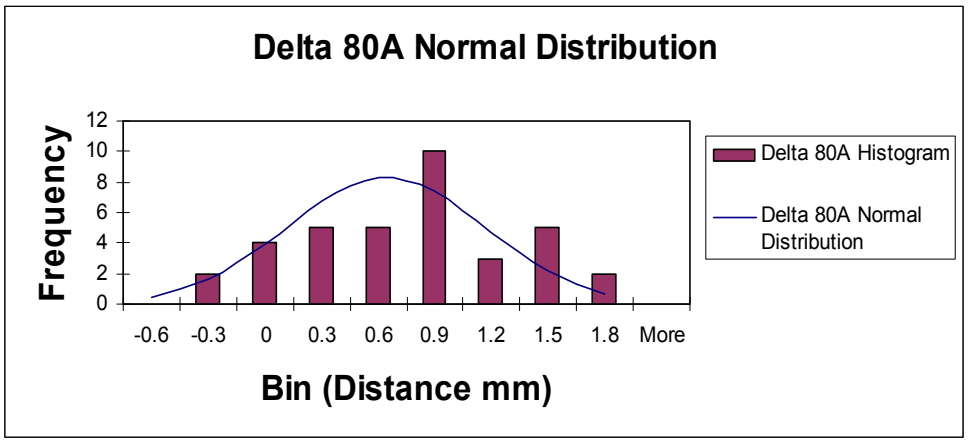

(f)

Figure 3.3(f) Normal distribution for $\Delta 80_A$.

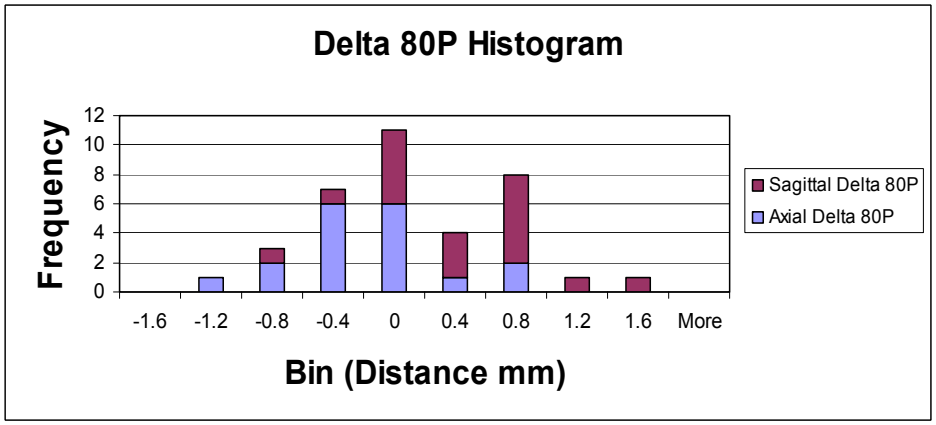

(g)

Figure 3.3(g) Histogram for $\Delta 80_P$

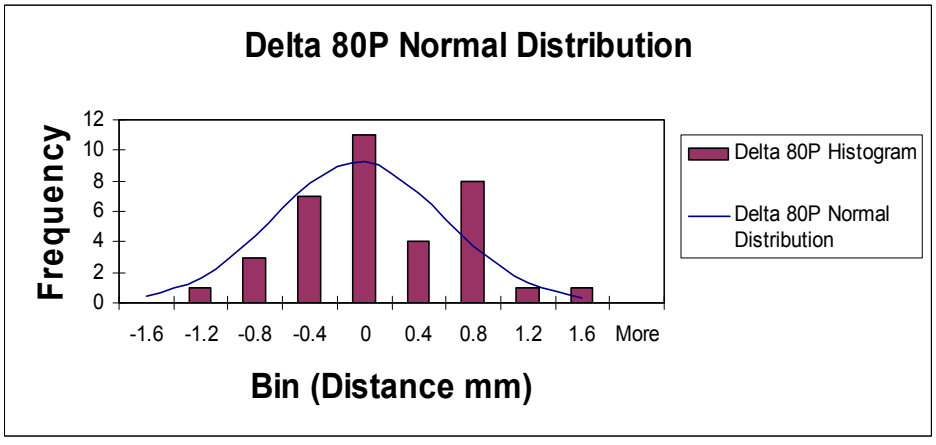

(h)

Figure 3.3(h) Normal distribution for $\Delta 80_P$.

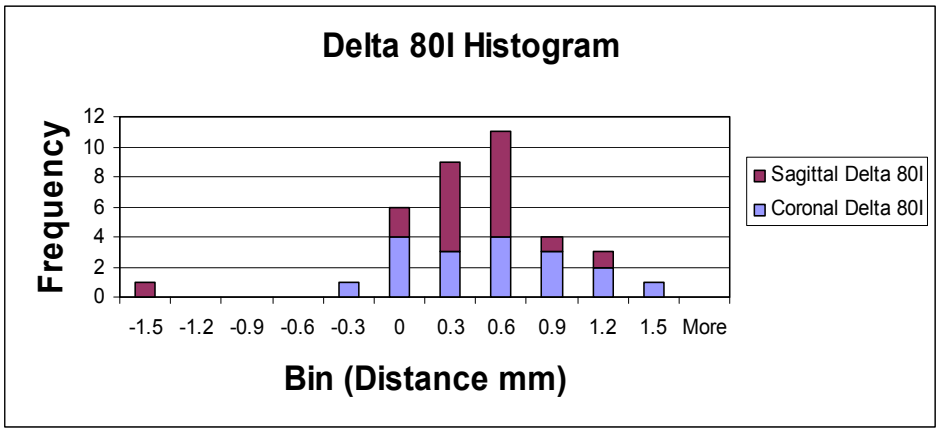

(i)

Figure 3.3 (i) Histogram for $\Delta 80_I$ metric.

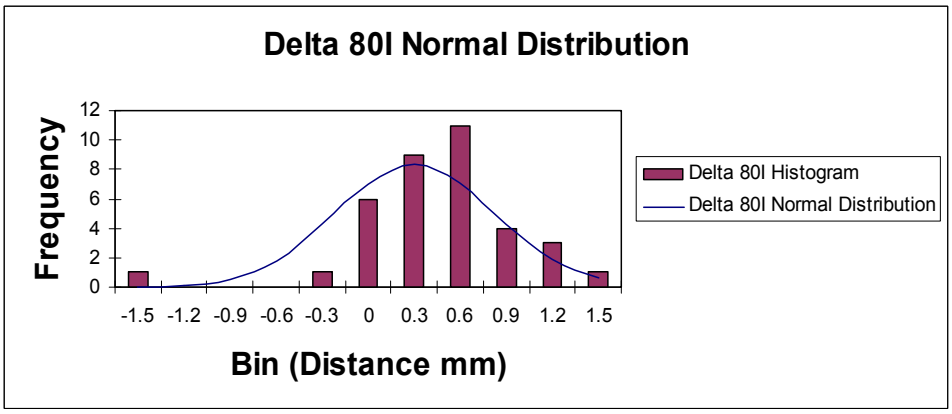

(j)

Figure 3.3(j) Normal distribution for $\Delta 80_I$ metric.

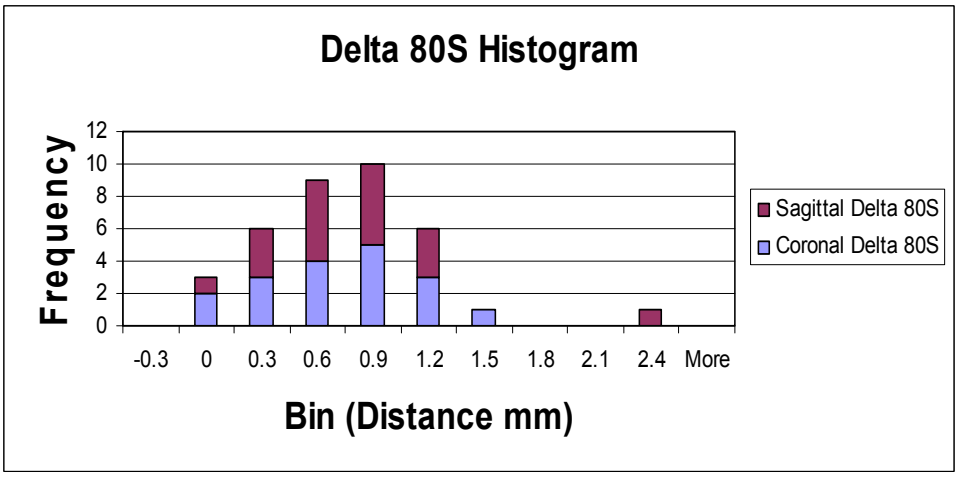

(k)

Figure 3.3(k) Histogram for $\Delta 80_S$ metric.

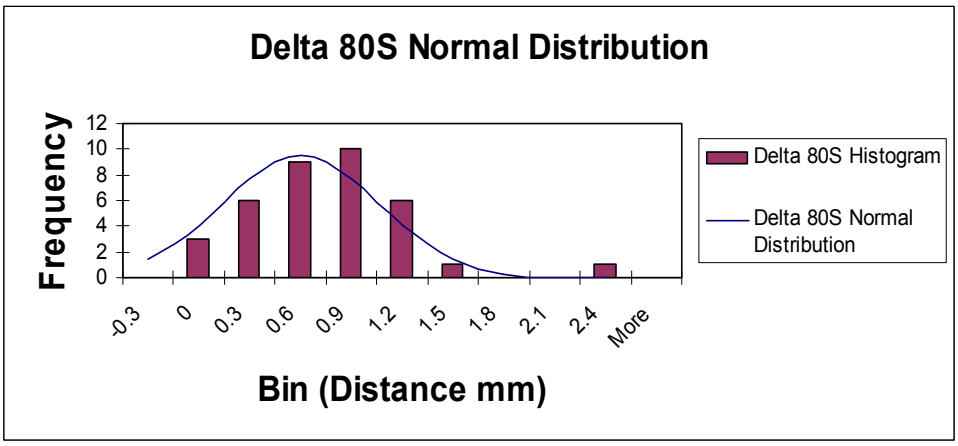

(l)

Figure 3.3(1) Normal distribution for $\Delta 80_S$ metric.

The mean error in the lateral direction was larger than the expected value of zero (1.28 mm in the lateral direction). Again this is believed to be due in part to the manual realignment of the phantom. The $\Delta 80$ metrics, except for $\Delta 80_L$ and $\Delta 80_P$, were all statistically significantly different than zero based on the standard error of the mean.

CHAPTER 4: CONCLUSIONS

4.1 SUMMARY OF RESULTS

MVCT image guided treatment using the TomoTherapy Hi•Art system can achieve positional alignment within -0.67 mm ± 0.93 mm, -0.36 mm ± 0.56 mm, and -0.15 mm ± 0.47 mm for an initial misalignment of 5mm from isocenter in the lateral, anterior-posterior, and superior-inferior directions respectively. The maximum error in the location of the 80% dose point was also seen in the lateral direction and was 3.62 mm. The larger errors in the lateral direction are believed to be due to play in the table motion and the manual realignment of the phantom to isocenter. During the study it was observed that the manual adjustment knobs and readout scale would indicate the table was moving, however, the couch was not fully engaged and did not move as much as indicated. This was not measured quantitatively, but could be seen on the rulers that were setup and used for misalignment of the phantom. For this study, manual realignment was done using only the adjustment knobs at the head and foot of the TomoTherapy couch and the readout scale on the table even though the rulers setup to determine the initial misalignment of the phantom were in place. The rulers were not used as a second check because in the clinic adjustments are made according to the TomoTherapy couch readout scale.

The results of this study could be affected by TomoTherapy imaging quality assurance (QA). During monthly QA, the accuracy of the machine isocenter lasers (virtual isocenter) is tested. The test images the TomoTherapy phantom and then manually registers the MVCT with the blank image containing a cross hair at isocenter. The results must be within ± 1 mm for both the lateral and vertical adjustments. The machine passed this test for the month the measurements for this study were taken. At the time of this study, the only imaging QA in place for the system was an airscan that was done daily to calibrate the detectors because the treatment

beam and imaging system utilize the same source and detectors. To help improve the results of this study a smaller FOV during CT scanning is recommended to help improve the resolution, using a 512 x 512 dose calculation grid in TomoTherapy, and weekly image registration QA should be done to test the realignment accuracy of the automatic image registration.

4.2 EVALUATION OF HYPOTHESIS

My hypothesis stated that SRS/SRT delivery using the MVCT image guidance feature of TomoTherapy could achieve positional dose delivery accuracy within 1mm for a cranial PTV in an anthropomorphic head phantom. My hypothesis was not proven as some measured errors were greater than 1mm for both the alignment and dose coverage metrics. It is believed that a reduction in the magnitude of measured errors may be seen on the new TomoTherapy couch which has automatic lateral adjustments.

4.3 CLINICAL RECOMMENDATIONS

Based on the AAPM Task Group 42 recommendation that an SRS system have a positional accuracy of ± 1mm, I would not currently recommend TomoTherapy for SRS using a non-invasive immobilization system, 1.98 mm dose voxel size, and manual lateral couch positioning. Applying the results of the study for PTV margin determination in conformal SRT, which recommends a margin of the systematic component of the total uncertainty plus one standard deviation, I would recommend using a margin of 2.19 mm laterally, 1.16 mm in the anterior-posterior, and 1.06 mm in the superior – inferior direction for SRT targets in the cranium treated on TomoTherapy. The margins are based on the dose errors ($\Delta 80_R$, $\Delta 80_A$, $\Delta 80_S$) which were determined to be 1.28 mm ± 0.91 mm, 0.64 mm ± 0.52 mm, and 0.60 mm ± 0.46

mm. This system would be recommended for SRT and hypofractionation (i.e. high-dose lung) particularly if an improvement in lateral error is seen with the new automated couch.

4.4 FUTURE WORK

Future work should include evaluation of the new automated couch (automated in lateral, anterior-posterior, and superior-inferior directions). Also, the use of an acceptance criterion for rescanning the phantom should be applied and evaluated to see how the accuracy and precision of treatment delivery is changed. Clinically, a weekly image registration QA procedure is going to be implemented; this test is going to use the MVCT TomoTherapy phantom intentionally misaligned by 2 cm laterally (left), 3 cm in the anterior-posterior, and 4 cm in the superior-inferior direction. Registration using the bone technique, standard resolution, and adjustments for translations and roll will be automatically done and results must agree within ± 1 mm. This study should be repeated to see if errors correlate with results of the image registration QA, as Vinci (2007) stated result correlated with the Winston-Lutz test in the anterior-posterior direction. It would also be useful to evaluate TomoTherapy for use with an irregularly shaped target volume and multiple targets in the cranium.

APPENDIX A: Linear attenuation coefficients, μ(cm^{-1}), physical densities, and electron densities of phantom materials versus "average human" (provided by CIRS).

	Average Soft Tissue			Average Bone Tissue			Spinal Discs			Spinal Cord			Average Brain Tissue		
Energy, MeV	ICRP 23, 1975	CIRS	Ratio %	ICRP 23, 1975	CIRS	Ratio %	Woodard et al (1986)	CIRS	Ratio %	ICRP 23, 1975	CIRS	Ratio %	ICRP 23, 1975	CIRS	Ratio %
0.04	0.2679	0.2678	99.96	0.7884	0.7887	100.04	0.3096	0.3097	100.03	0.2769	0.2768	99.96	0.2791	0.2791	100
0.06	0.2087	0.2091	100.19	0.4244	0.4242	99.95	0.2287	0.2288	100.04	0.2125	0.2124	99.95	0.2135	0.2138	100.14
0.08	0.1871	0.1876	100.27	0.3251	0.3248	99.91	0.2014	0.2015	100.05	0.1895	0.1894	99.95	0.1902	0.1907	100.26
0.1	0.1742	0.1748	100.34	0.2822	0.2819	99.89	0.1862	0.1863	100.05	0.1762	0.1761	99.94	0.1767	0.1772	100.28
0.15	0.1538	0.1544	100.39	0.2344	0.2341	99.87	0.1634	0.1635	100.06	0.1552	0.1552	100	0.1557	0.1562	100.32
0.2	0.1401	0.1406	100.36	0.2098	0.2095	99.86	0.1486	0.1487	100.07	0.1414	0.1413	99.93	0.1418	0.1422	100.28
0.4	0.1086	0.109	100.37	0.1605	0.1602	99.81	0.115	0.1151	100.09	0.1095	0.1095	100	0.1098	0.1102	100.36
0.6	0.0917	0.092	100.33	0.1351	0.1349	99.85	0.0971	0.0971	100	0.0924	0.0924	100	0.0927	0.093	100.32
0.8	0.0805	0.0808	100.37	0.1186	0.1184	99.83	0.0852	0.0853	100.12	0.0812	0.0811	99.88	0.0814	0.0817	100.37
1	0.0724	0.0726	100.38	0.1066	0.1064	99.81	0.0766	0.0767	100.13	0.073	0.0729	99.86	0.0731	0.0734	100.41
1.5	0.0589	0.0591	100.34	0.0868	0.0866	99.77	0.0624	0.0624	100	0.0594	0.0594	100	0.0595	0.0597	100.34
2	0.0505	0.0507	100.4	0.0746	0.0745	99.87	0.0535	0.0536	100.19	0.051	0.051	100	0.0511	0.0513	100.39
4	0.0347	0.0348	100.29	0.0521	0.052	99.81	0.0369	0.0369	100	0.0351	0.035	99.72	0.0352	0.0352	100
6	0.0282	0.0282	100	0.0431	0.043	99.77	0.0301	0.0301	100	0.0285	0.0285	100	0.0286	0.0286	100
8	0.0247	0.0247	100	0.0383	0.0383	100	0.0265	0.0265	100	0.025	0.0249	99.6	0.0251	0.025	99.6
10	0.0225	0.0225	100	0.0355	0.0355	100	0.0242	0.0242	100	0.0227	0.0227	100	0.0229	0.0228	99.56
15	0.0196	0.0195	99.49	0.0319	0.032	100.31	0.0213	0.0212	99.53	0.0198	0.0198	100	0.02	0.0199	99.5
20	0.0182	0.0181	99.45	0.0305	0.0305	100	0.0199	0.0199	100	0.0185	0.0185	100	0.0186	0.0185	99.46
30	0.0171	0.017	99.42	0.0296	0.0296	100	0.0189	0.0188	99.47	0.0174	0.0174	100	0.0176	0.0174	98.96
Density, g/cm^3	1.03	1.055		1.577	1.6		1.1	1.131		1.037	1.07		1.04	1.069	
Electron Density, $*10^{23}$, cm^{-3}	3.421	3.434	100.38	5.035	5.028	99.86	3.621	3.624	100.08	3.449	3.448	99.97	3.458	3.47	100.35

APPENDIX B: Supplemental Data on TomoTherapy's Automated Lateral Couch

Two sets of measurements (7/22/2010 and 7/23/2010) were taken on the upgraded TomoTherapy Hi-Art system software version 4.0. Measurements were taken for a limited subset of the original points (no offset, point4, and point 6). The CT scans, contours, and constraints from the original study were used for treatment planning. The results in this section are for the phantom visually aligned to isocenter, MVCT scanned then automatic adjustments applied for nominal position, intentionally offset, MVCT scanned and realigned using the automatic adjustments, and then MVCT scanned for setup verification. An acceptance criterion of ± 1 mm, 1° was utilized (additional CT scans were not required for any of the measurements, acceptance criteria was met every time).

Measurement Set 1		Axial Film Plane						Coronal Film Plane						Sagittal Film Plane					
Sample Space Point	Offset Coordinates	$\Delta 80_R$	$\Delta 80_L$	$\Delta 80_A$	$\Delta 80_P$	Δc_{RL}	Δc_{AP}	$\Delta 80_R$	$\Delta 80_L$	$\Delta 80_S$	$\Delta 80_I$	Δc_{RL}	Δc_{SI}	$\Delta 80_A$	$\Delta 80_P$	$\Delta 80_S$	$\Delta 80_I$	Δc_{AP}	Δc_{SI}
0	(0,0,0)	0.63	0.90	1.39	0.54	0.34	-0.37	1.00	0.62	0.52	0.68	-0.80	0.07	0.99	0.53	0.61	0.88	-0.24	0.15
4	(5,5,5)	1.07	0.98	1.62	0.15	-0.54	-0.57	1.85	-0.05	-0.05	1.79	-1.54	0.95	0.85	0.31	-0.28	1.87	-0.28	1.05
6	(-5,-5,-5)	1.78	0.84	1.87	0.18	-0.80	-0.92	2.04	-0.26	0.12	1.40	-1.58	0.63	0.99	0.28	0.11	1.09	-0.48	0.50
0	(0,0,0)	2.24	0.78	1.77	0.00	-0.77	-0.91	1.71	0.34	0.60	1.25	-1.17	0.28	0.86	-0.08	0.23	0.95	-0.55	0.41
6	(-5,-5,-5)	1.77	0.09	1.43	0.11	-0.92	-0.74	1.69	-0.59	0.70	1.61	-1.69	0.27	1.00	0.20	0.31	1.29	-0.52	0.42

Measurement Set 2		Axial Film Plane						Coronal Film Plane						Sagittal Film Plane					
Sample Space Point	Offset Coordinates	$\Delta 80_R$	$\Delta 80_L$	$\Delta 80_A$	$\Delta 80_P$	Δc_{RL}	Δc_{AP}	$\Delta 80_R$	$\Delta 80_L$	$\Delta 80_S$	$\Delta 80_I$	Δc_{RL}	Δc_{SI}	$\Delta 80_A$	$\Delta 80_P$	$\Delta 80_S$	$\Delta 80_I$	Δc_{AP}	Δc_{SI}
0	(0,0,0)	1.95	0.29	1.58	-0.03	-1.03	-0.79	1.95	0.37	-0.51	2.04	-1.54	1.34	1.23	0.39	0.73	1.04	-0.45	0.22
4	(5,5,5)	1.86	0.52	1.60	0.22	-0.80	-0.68	1.49	0.500	0.31	1.65	-0.96	0.62	1.08	-0.23	0.23	1.59	-0.60	0.59
6	(-5,-5,-5)	1.59	0.24	1.47	-0.18	-0.80	-0.68	1.51	0.65	0.43	1.05	-0.94	0.27	0.73	0.68	0.20	1.47	-0.14	0.58
4	(5,5,5)	1.67	0.54	1.56	-0.21	-0.92	-0.78	1.12	0.39	0.41	1.16	-0.99	0.41	0.86	0.21	0.40	1.22	-0.37	0.31

The differences (mean ± standard deviation) in Δc were -0.97 ± 0.46 mm (range: -1.69 to 0.34 mm), -0.56 ± 0.22 mm (range: -0.92 to -0.14 mm), and 0.50 ± 0.33 mm (range: 0.07 to 1.34 mm). The standard deviation of the positional alignment error (Δc) is a measure of the reproducibility of alignment with the planning CT using the MVCT image guidance. The reproducibility (2σ) of TomoTherapy MVCT alignment was within 0.92 mm. The mean displacement of the measured 80% dose points in millimeters were 1.61 ± 0.41 (range: 0.63 to 2.24), 0.40 ± 0.41 (range: -0.55 to 0.98), 1.29 ± 0.36 (range: 0.73 to 1.87), 0.17 ± 0.26 (range: -0.23 to 0.68), 0.28 ± 0.33 (range: -0.51 to 0.73), and 1.34 ± 0.37 (range: 0.68 to 2.04).

VITA

Before entering Louisiana State University's Medical Physics and Health Physics graduate program, Catherine took two years off after earning an undergraduate degree in Biophysics while playing collegiate volleyball. During that time, she taught high school physics and geometry at her alma mater. Then she worked for the bulk terminals division of Kinder Morgan, Inc., where she learned about the environmental permitting processes for building terminals which transport and store dry bulk goods. Catherine's appreciation of physics and medicine was neglected in both of these jobs, and so she made the decision to return to school. While doing her research in medical physics, Catherine made the decision to further pursuit her genuine interest in the helping people on a daily basis and investigation of feasible ways to improve cancer treatment by enrolling in medical school. She is currently enrolled in her first year of medical school.